공학석사 학위논문

Analysis of photoconductivity and effects of CuI as a templating layer in fullerene based Schottky solar cells

Fullerene을 이용한 Schottky 태양전지에서 광전도성 및 배향층으로서의 CuI 효과 분석

2014년 2월

서울대학교 대학원

재료공학부

최 민 수

Analysis of photoconductivity and effects of CuI as a templating layer in fullerene based Schottky solar cells

지도 교수 김 장 주

이 논문을 공학석사 학위논문으로 제출함

2014 년 2 월

서울대학교 대학원

재료공학부

최 민 수

최 민 수 의 석사 학위논문을 인준함

2014 년 2 월

위 원 장 서 용 석 (인)

부위원장 김 장 주 (인)

위 원 남 기 태 (인)

Abstract

Analysis of photoconductivity and effects of CuI as a templating layer in fullerene based Schottky solar cells

Min-Soo Choi

Department of Materials Science and Engineering

The Graduate School

Seoul National University

In this thesis, the bulk-ionized photoconductivity of fullerenes in the Schottky solar cells has been investigated by three experiments. First, comparison of C_{60} and C_{70} is carried out. Since C_{70} has larger exciton generation rate (more overlap with solar spectrum about 2.3 times) than C_{60}, photoconductivity of C_{70} is higher than C_{60}. But, increase in photoconductivity is only 1.7 times, due to difference in thermalization distance. It is discussed with X-ray scattering data.

Then, work function of electrode is changed with interfacial layers. Linear dependence of photocurrent on electric field is observed and changing the interfacial layer to modify work functions of electrode leads to variation of the built-in potential (V_{bi}). These have been confirmed by calculations using

equation from photoconductivity and capacitance-voltage (C-V) characteristics.

Third experiment is inserting CuI as a templating layer. In the images of grazing incidence wide angle x-ray scattering (GIWAXS), C_{60} on CuI layer shows higher crystallinity than C_{60} on ITO substrate. The preferred orientation is FCC(111) which is closed packing plane for vertical direction to substrate. This effect makes photoconductivity increase by 43.8% in MoO_3 used and by 93.5% in ReO_3 used Schottky solar cells.

Finally, based on these results, high efficiency solar cells with 6.2% have been achieved.

Keywords: photoconductivity, fullerene, Schottky slar cell, built-in potential, capacitance-voltage characteristic, CuI, templating, low-donor concentration solar cell

Student Number: 2012-20638

Contents

List of figures

List of Tables

Chapter 1 Introduction

1.1 Motivation

Fullerene derivatives are typical acceptor materials for organic photovoltaic cells due to their appropriate energy levels to form charge transfer state with various donor materials and high electron mobility. [1] One of the simple structures of fullerene derivatives is C_{60}, as shown Figure 1.1. HOMO, LUMO and Fermi level of C_{60} are located at -6.2 eV, -4.0 eV and -4.5 eV from vacuum level, respectively. [1, 2]

As known, C_{60} forms intermolecular charge transfer exciton in solid film, leading to the extra absorption from 400 to 600 nm as shown in Figure 1.1. [3] The CT exciton in bulk of C_{60} can be dissociated easily by internal electric field. This bulk-ionization is called “photoconductivity”, a linear function of the field. [4] It is observed in J-V characteristics of planar heterojunction OPVs, with linear dependence of photocurrent on applied voltage in range from reverse voltage to small forward voltage.

To investigate photoconductivity of fullerenes, here, Schottky solar cells are suggested. In Schottky solar cell, photo-active layer consist of acceptor without donor material and interface between donor and acceptor does not exist. There is neither exciton diffusion to the interface nor dissociation at the interface, which occur in conventional OPV. All of the photocurrent is generated from the CT state of fullerene, not donor-acceptor interface. This means the origin of photocurrent in the Schottky solar cells is photoconductivity of fullerenes.

In this thesis, three questions are researched;

How about C_{70}?

How to change V_{OC}?

How about increasing crystallinity?

First, comparison of C_{60} and C_{70} is performed. C_{70} has similar molecular structure and crystal structure. However, absorption spectrum is different with that of C_{60}. Because overlap integral with solar spectrum is 2.3 times larger than that of C_{60}, photon absorption is 2.3 times larger. Accordingly, exciton generation rate is 2.3 times larger than that of C_{60}. This is related with photoconductivity of C_{70} which is higher than that of C_{60}. But, increase in photoconductivity is only 1.7 times, due to difference in thermalization distance. It is discussed with X-ray scattering data in **Chapter 2**.

In **Chapter 3**, the Schottky junction in the Schottky solar cells is studied by changing work function of electrode. The work function of the electrode can be modified by inserting interfacial layers of MoO_3 and ReO_3. Linear dependence of photocurrent on electric field is observed and changing the interfacial layer to modify work functions of electrode leads to variation of the built-in potential (V_{bi}). These have been confirmed by calculations from photoconductivity and capacitance-voltage (C-V) characteristics.

Last question is handled in **Chapter 4**. Cryltallinity is controlled with CuI as a templating layer. In the general OPV, high mobility and fill factor can be obtained from high crystallinity. However, CuI is known as a templating material for donors, such as metal-phthalocyanines, but effect of CuI on fullerene is not researched yet. [5-7] Here, effect of CuI on fullerene is researched. In the images of grazing incidence wide angle x-ray scattering

(GIWAXS), C_{60} on CuI layer shows higher crystallinity than C_{60} on ITO substrate. The preferred orientation is FCC(111) which is closed packing plane for vertical direction to substrate. This effect makes photoconductivity increase by 43.8% in MoO_3 used and by 93.5% in ReO_3 used Schottky solar cells.

Finally, based on these results, high efficiency solar cells with 6.2% have been achieved in **Chapter 5**.

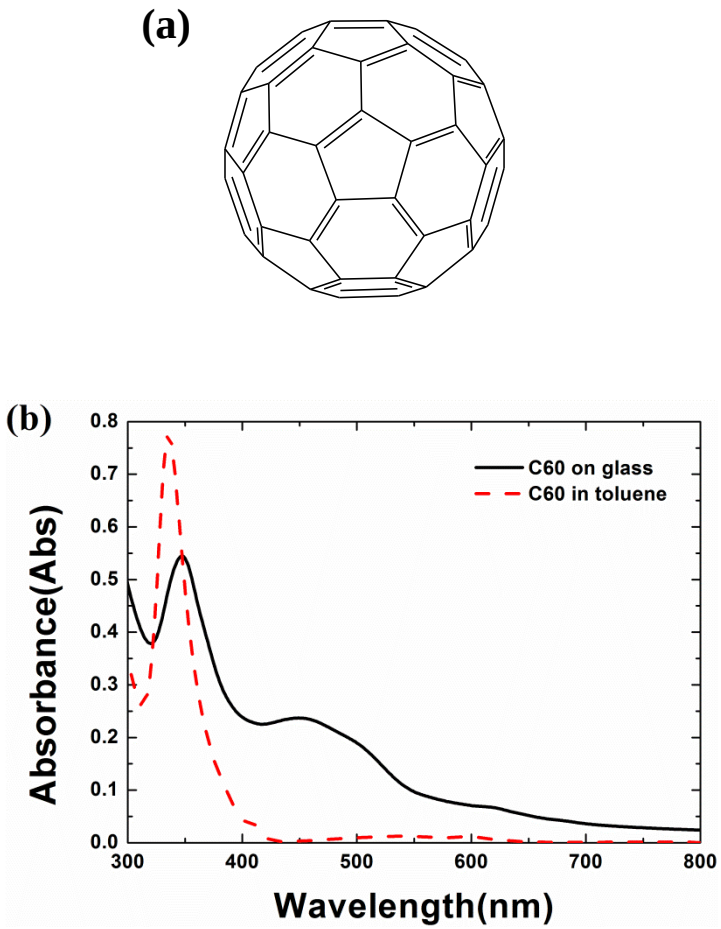

Figure 1.1 (a) Structure of C_{60} molecule. (b) Absorption spectra of C_{60}. Solid line represents absorption of C_{60} film and dashed line represents absorption of C_{60} in toluene.

1.2 Principle of Organic Photovoltaic Cells

Organic photovoltaic cells consist of metallic electrodes at both sides and organic active layers between them. When light is illuminated to organic layer, electrons in HOMO level are excited by absorbing photon and jump to LUMO level remaining holes in HOMO level. The Electrons and the holes bounded by Coulombic interaction are called exciton. These excitons cannot be easily dissociated due to large exciton binding energy (around 0.1~0.2 eV). In order to be dissociated, excitons should diffuse to interface between donor and acceptor. Since there is local field at the interface, excitons which arrived at the interface can be easily dissociated. Then, the electrons and the holes drift by internal electric field and collected at electrode.

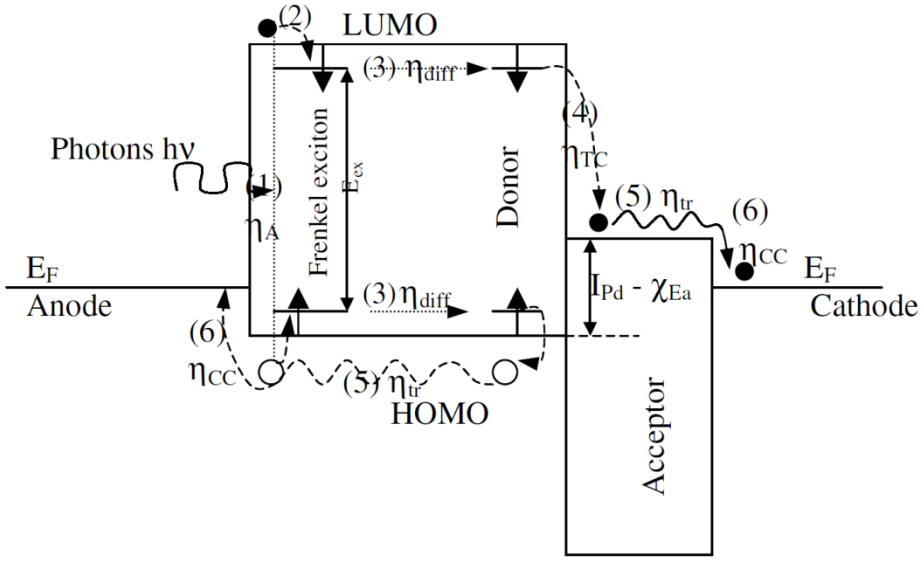

Figure 1.2 Mechanisms of photocarrier generation in organic photovoltaic cells. [8]

1.3 Photoconductivity

In organic solar cells, excitons are generated by absorbing photons. These excitons should overcome their Coulomb interaction energy in order to generate free charge carriers. If excitons cannot undergo dissociation process, it returns to ground state without producing free charge carriers. This process is called geminate recombination, which are major photocurrent loss mechanism in organic solar cells. The geminate recombination was described firstly by Onsager. [9] Onsager proposed the theory of geminate recombination which gives the probability for thermalized charge pairs to dissociate under influence of electric field in the isotropic system containing a low concentration of charge pairs. Under thermal equilibrium, electrons can move with thermal energy, *kT* and bounded by Coulombic force. Then, the balance between the thermal energy of electron and Coulomb interaction energy is described as

$$\frac{e^2}{4\pi\varepsilon_r\varepsilon_0 r_c} = kT \tag{1.1}$$

where *e* is element of charge, ε_r is the dielectric constant of material and ε_0 is vacuum permittivity. [3] Here, the r_c is Coulombic capture radius,

$$r_c = \frac{e^2}{4\pi\varepsilon_r\varepsilon_0 kT}\,. \tag{1.2}$$

If the thermalization distance, r_0 of electron is longer than Coulombic capture radius of excitons, excitons are dissociated into free charges, which represented the bulk ionization of excitons. Here, the probability of dissociation is described as

$$\Phi = \exp\left(-\frac{r_c}{r_0}\right). \tag{1.3}$$

When voltage is applied, internal electrical field distributes in organic layer and probability of dissociation becomes larger. Using analytic form of Onsager theory, dissociation probability of excitons is described as

$$\Phi(F) = \left(1 + \frac{er_c}{2kT}F\right)\exp\left(-\frac{r_c}{r_0}\right) \tag{1.4}$$

where F represents electric field distributes in the organic layer. This equation is available at low electric field region. It indicates that bulk ionization probability shows linear dependence of the internal electric field

1.4 Schottky Solar Cells

Generally, there are two types of contacts between metallic electrode and semiconductor. One is Ohmic contact and another is Schottky contact. Ohmic contact has no barrier for the flow of charge carriers in both directions. In this case, current increases linearly with increasing voltage, showing Ohm's law.

Schottky contact is different. Potential barrier exists between metallic electorde and semiconductor, called Schottky barrier. Figure 1.3 shows the Schottky barrier between metal and n-type semiconductor. Since work function of metal is larger than semiconductor, electrons start to flow from the semiconductor into the metal until Fermi energies of both sides are same. Then, the metal is charged negatively and a potential barrier is formed.

Current-voltage characteristic of Schottky contact is different with Ohmic contact. When Metal is contacted to negative electrode and semiconductor is contacted to positive electrode (reverse bias), potential of metal becomes higher and depletion width is increased. There is only diffusion current. However, metal is in contact with positive electrode and semiconductor is in contact with negative electrode (forward bias), potential of semiconductor goes higher and depletion width is decreased. Therefore, this contact shows diode current characteristic.

In Schottky contact, internal electric field distributes near the Schottky barrier which can be used as solar cell. When exciton is generated, it can be dissociated by internal electric field. This system is called Schottky solar cell, as shown Figure 1.4.

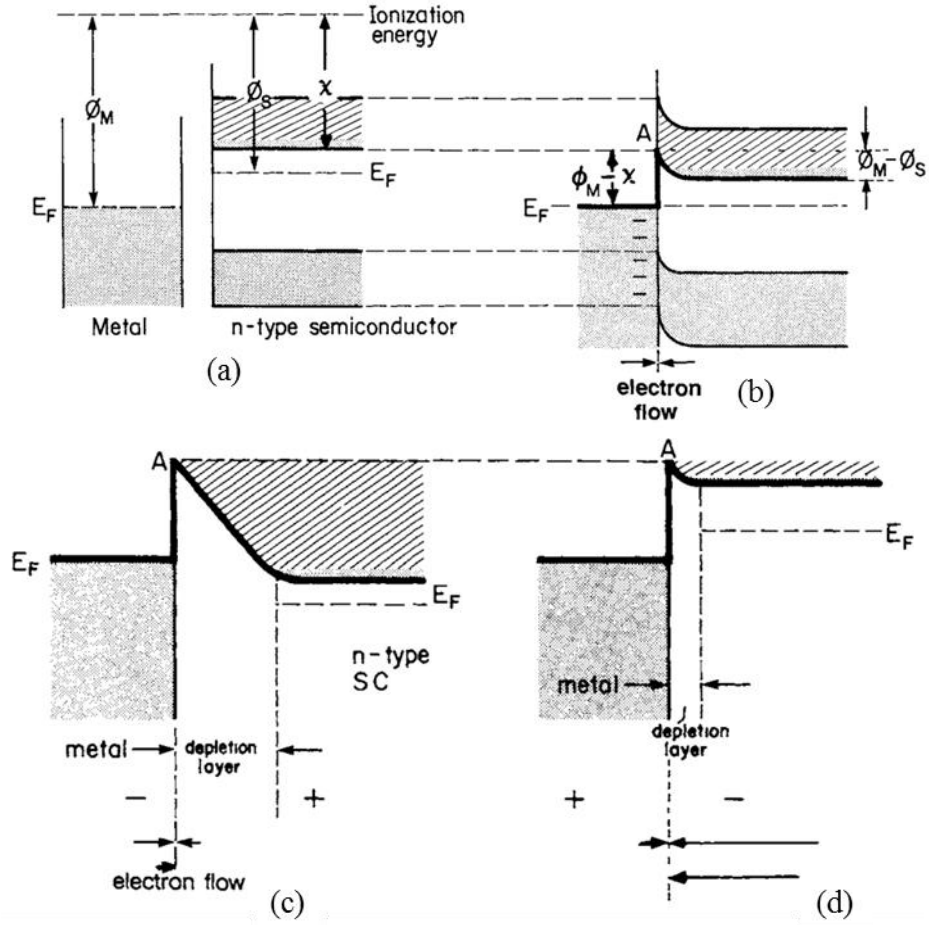

Figure 1.3 Energy bands for a metal and an n-type semiconductor (a) before contact, (b) after contact, (c) with reverse bias and (d) with forward bias. The number of electrons that flow in both directions and the net current is indicated by the length of the arrows. The potential barriers are marked by heavy lines. [10]

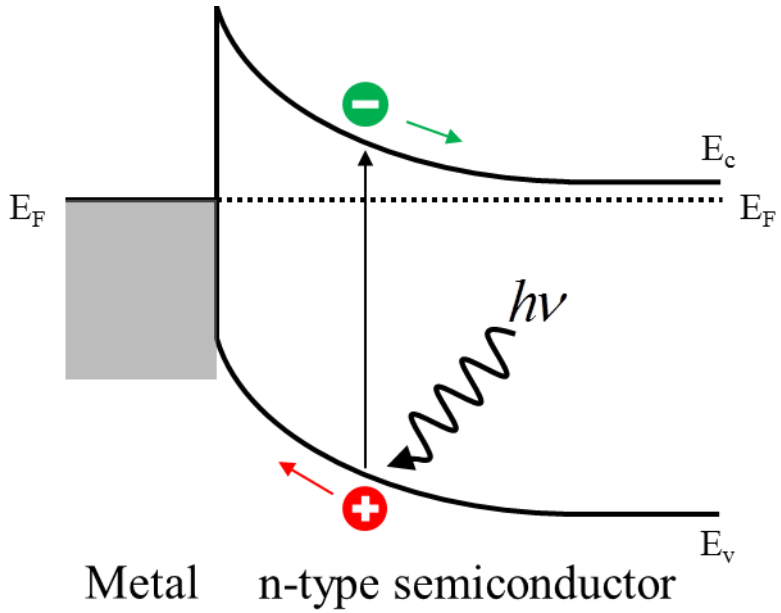

Figure 1.4 Energy band diagram of Schottky solar cell under illumination. Generated exciton is dissociated by internal electric field.

Chapter 2 Comparison of C_{60} and C_{70}

2.1 Introduction

Fullerene is known as n-type material and non-doped C_{60} has charge carriers of which concentration is about 3×10^{16} cm^{-3}. [11] Due to large charge carrier concentration, band bending occurs in C_{60} layer and depletion width in fullerene layer is reported as 42nm and 55nm. [4, 12] Fullerene based Schottky solar cell is possible as shown in Figure 2.1.

Here, comparison of C_{60} and C_{70} is performed. C_{70} has similar molecular structure and crystal structure. However, absorption spectrum is different with that of C_{60}. Because overlap integral with solar spectrum is 2.3 times larger than that of C_{60}, photon absorption is 2.3 times larger. Accordingly, calculated exciton generation rate is 2.3 times larger than that of C_{60}. This is related with photoconductivity of C_{70} which is higher than that of C_{60}. But, increase in photoconductivity is only 1.7 times, due to difference in thermalization distance. It is discussed with X-ray scattering data.

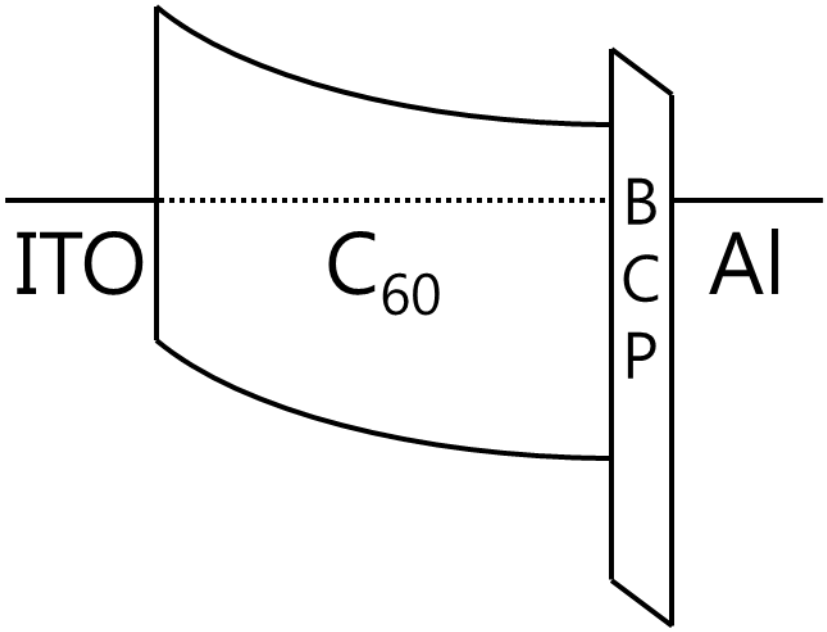

Figure 2.1 Energy band diagram of fullerene based Schottky solar cell. Electric field distributes whole of the layer. Energy level is from **chapter 3**.

2.2 Experiments

Schottky solar cells has the following structure: indium tin oxide (ITO) (150 nm) / C_{60} or C_{70} (60 nm) / BCP (8 nm) / AL (100 nm). Device structure is shown in Figure 2.2.

The ITO-coated glass substrate was successively cleaned with acetone and isopropyl alcohol. The substrate was exposed to UV-O_3 for 15 min before use. All the organic layers were deposited using thermal evaporation at the base pressure of ca. 10^{-7} torr with a rate of 1 Å/s without breaking the vacuum. The devices had active areas of 2×2 mm^2. A patterned insulator on the ITO and the top cathode deposited through a shadow mask defined the cell area. After fabrication, the devices were encapsulated using the epoxy resin in N_2 environment. The photovoltaic properties of the device were measured with an AM 1.5G 100 mW/cm^2 solar simulator (300 W Oriel 69911A) light source and a source measurement unit (Keithley 237). The measurement set up was calibrated with a National Renewable Energy Laboratory-certified reference Si-solar cell covered with a KG-5 filter before every measurement. The UV-Vis absorption spectra of films were recorded with a VARIAN Cary 5000 UV-vis spectrophotometer. The crystalline properties were investigated by synchrotron x-ray scattering measurements at 5A x-ray scattering beamline for materials science of Pohang Light Source II (PLS-II). The x-ray wavelength was 1.071 Å (11.58 keV). The films were deposited on ITO substrates.

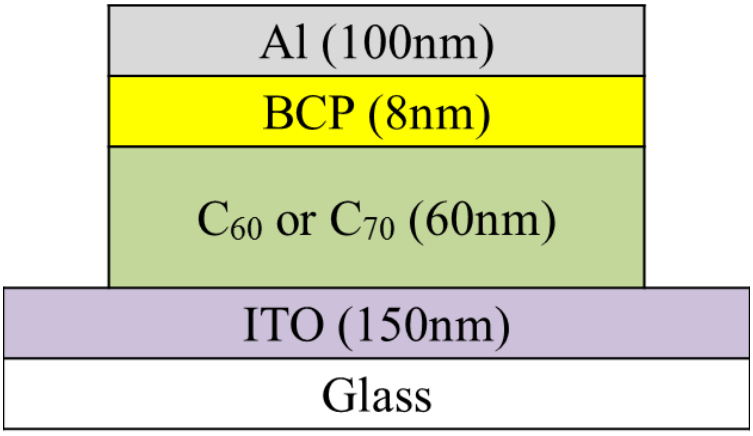

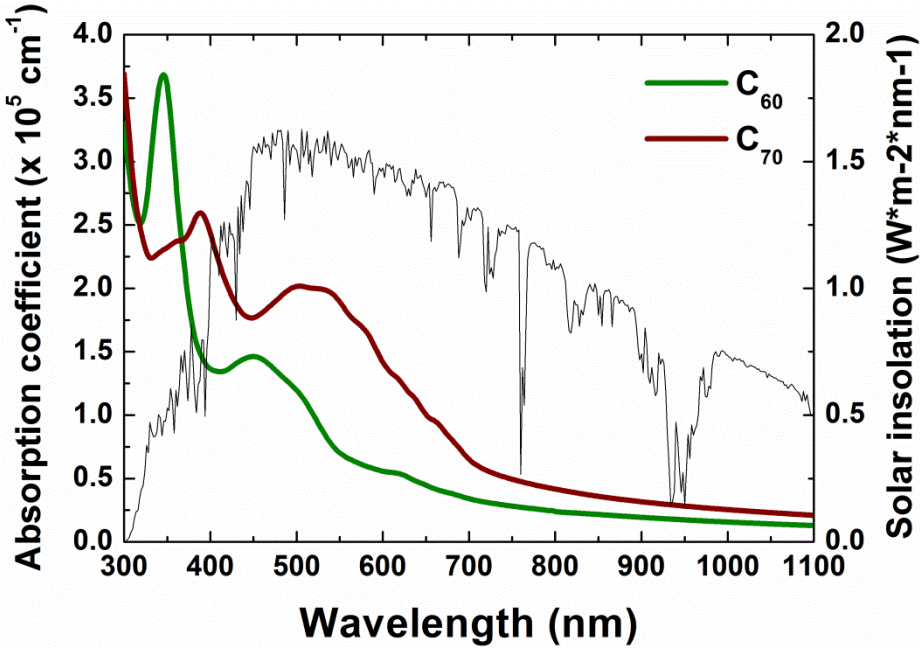

Figure 2.2 Device structure of fullerene based Schottky solar cells and absorption spectra of C_{60} and C_{70} with solar radiation spectrum

2.3 Result and Discussion

Figure 2.3 shows J-V curves and IPCE spectra of fullerene based Schottky solar cells. In J-V curves, photocurrents of two devices increase linearly with increasing V_{app}. It means that photocurrent is generated by photoconductivity in fullerene bulk. Slope of J-V curves indicate field dependence of photoconductivity on V_{app} and large slope means that is large, in other word, bulk-ionization yield is high. At the same condition (same internal electrical field and same light intensity), more photocurrent is generated when bulk-ionization yield is high.

C_{60} used and C_{70} used device show different slope of J-V curves and different V_{OC}. In Figure 2.3 (a), slope of C_{70} used device is steeper than that of C_{60} used. It is due to difference in exciton generation rate, calculated from different absorption spectra, shown in Figure 2.2 and summarized in Table 2.3. Moreover, difference in V_{OC} can be also explained with absorption spectra. As absorption wavelength of C_{70} is longer than C_{60}, it indicates band gap is smaller than C_{60}. Therefore, V_{OC} of C_{70} is smaller than C_{60}.

In Figure 2.3 (b), absorption spectra of C_{60} and C_{70} are reflected in IPEC spectra. Shoulder at 620nm is shown in both of absorption spectrum and IPCE of C_{60}. Peak in range of 450~700 nm is shown in both of absorption spectrum and IPCE, in C_{70} case.

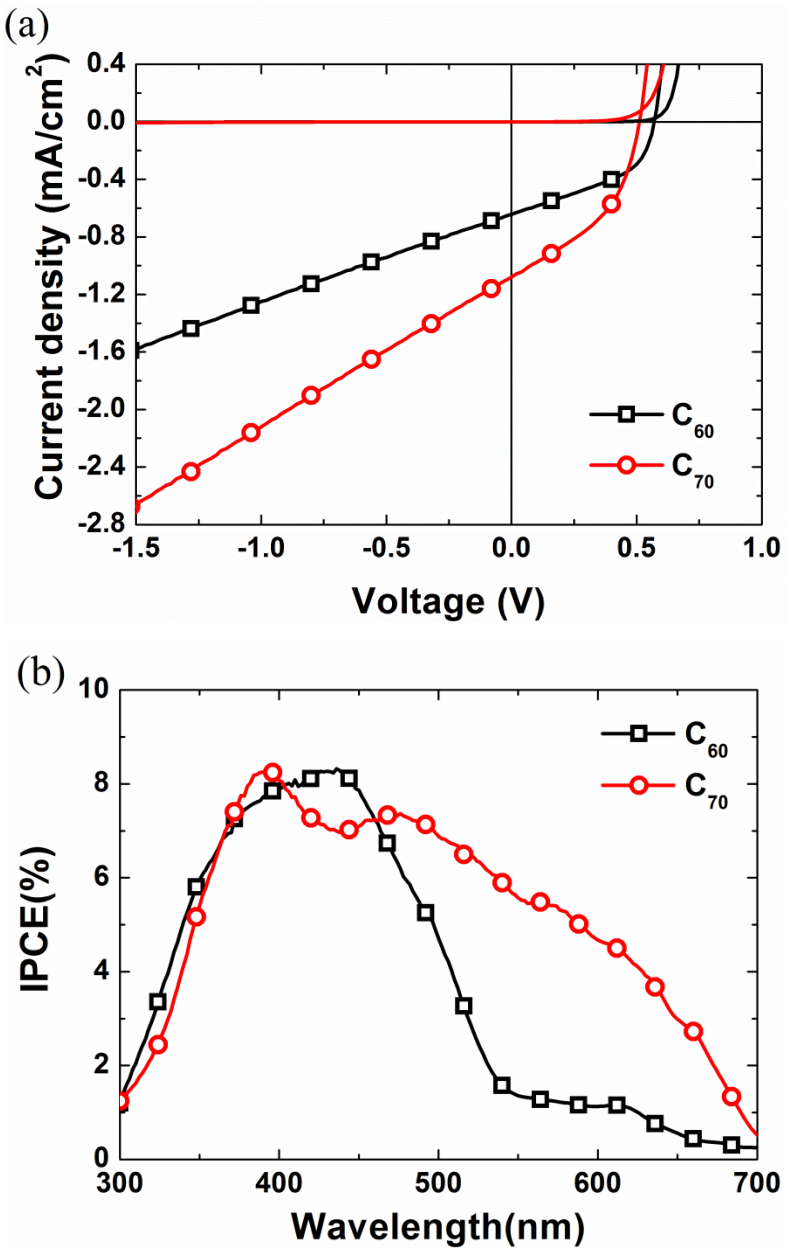

Figure 2.3 (a) J-V curves and (b) IPCE spectra of fullerene based Schottky solar cells

Table 2.1 The photovoltaic properties of fullerene based Schottky solar cells. C_{60} and C_{70} are used as active materials.

Acceptor	PCE (%)	J_{SC} (mA/cm^2)	V_{OC} (V)	Fill Factor
C_{60}	0.16	0.64	0.57	0.44
C_{70}	0.24	1.08	0.51	0.43

Here, J-V curves are interpreted by fitting with equation from photoconductivity. In solar cells, photocurrent is summation of dark current and photo-generated current. In dark condition without light illumination, current is governed by diode equation due to Schottky barrier. It is written as

$$J_d = J_s\left[\exp\left(\frac{eV_{app}}{nkT}\right)-1\right] \tag{2.1}$$

where, J_S is dark saturation current, e is Coulomb's constant, V_{app} is applied voltage, n is ideality factor, k is Boltzmann constant and T is temperature. [13]

In J-V curves, photocurrent is a linear function of V_{app}; therefore it can be described as

$$J_{ph} = I - SV_{app} \tag{2.2}$$

where I is intercept and S is slope of J-V curves, here, I means fitted J_{SC}.

Then, photocurrent which summation of dark current and photo-generated current is described as

$$J = J_{dark} - J_{ph} = J_s\left[\exp\left(\frac{eV}{nkT}\right)-1\right]+\left(I-SV\right). \tag{2.3}$$

Using equation (2.3), fittings of J-V curves of fullerene based Schottky solar cells are performed, shown in Figure 2.4.

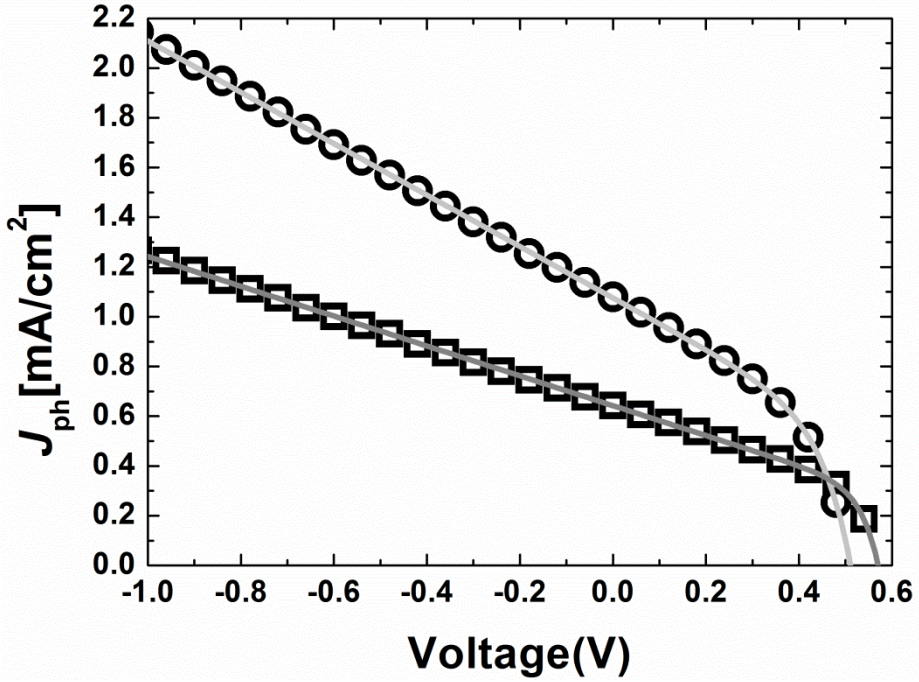

Figure 2.4 Fitting of J-V curves. Experimental results are represented by squares (C_{60}) and circles (C_{70}). The gray lines indicate fitted lines.

Table 2.2 Fitted parameters from J-V curves.

Acceptor	J_S (mA/cm^2)	S (mA/cm^{2}V)	I (mA/cm^2)	n	J_{SC} (mA/cm^2)
C_{60}	8.68×10^{-8}	0.600	0.642	1.517	0.64
C_{70}	1.33×10^{-7}	1.03	1.08	2.458	1.08

Here, fitted intercepts are well matched with J_{SC}.

However, photo-generated current is from the photo-ionization in bulk. It is a function of bulk-ionization yield and exciton generation rate, described as

$$J_{ph} = eG\Phi(V). \tag{2.4}$$

where G is exciton generation rate. [4] As explained in equation (1.4), bulk-ionization yield is

$$\Phi(F) = \left[1 + \frac{er_c}{2kT}F\right]\exp\left(-\frac{r_c}{r_0}\right), \tag{2.5}$$

and the field can be replaced by V_{app}, thickness of organic layer and V_{bi}. With a combination of equations, photo-generated current is written as

$$J_{ph} = eG\Phi(V) = eG\left[1 + \frac{er_c}{2kT}\left(\frac{V_{bi} - V_{app}}{d}\right)\right]\exp\left(-\frac{r_c}{r_0}\right). \tag{2.5}$$

Exciton generation rate, G is calculated by transfer matrix method. [14] The number of excitons generated in 60nm of active layer is summarized in Table 2.3.

Photo-generated current is from the photo-ionization in bulk, a combination of equations leads;

$$J_{ph} = I - SV_{app} = eG\left[1 + \frac{er_c}{2kT}\left(\frac{V_{bi} - V_{app}}{d}\right)\right]\exp\left(-\frac{r_c}{r_0}\right). \quad (2.6)$$

From the equation above, thermalization distance can be calculated with ε_r is 4.5 and T is 300 K.

$$r_0 = -\frac{r_c}{\ln\left(\frac{2kTd}{e^2 \mathrm{G} r_c} S\right)} \quad (2.7)$$

Table 2.3 Calculated parameters from J-V curves and absorption spectra.

Acceptor	Exciton generation rate G (#/cm^2·s)	S / G (#/#·V)	Thermalization distance r_0 (nm)	Zero field Quantum yield
C_{60}	3.294×10^{16}	0.1137	3.44	0.02757
C_{70}	7.444×10^{16}	0.08638	3.20	0.02093

S / G is conversion ratio, meaning that how many electrons can be generated by one photon. As photoconductivity is a function of applied voltage, conversion ratio is also a function of applied voltage too.

Difference in conversion ratio can be explained with thermalization distance. Thermalization distance of C_{60} is longer than that of C_{70}, due to size of molecule is different. Size of C_{60} molecule is smaller than that of C_{70}, therefore lattice constants are different. In Figure 2.5, peak of FCC(111) is observed, at Q=0.770 (C_{60}) and Q=0.734 (C_{70}). From X-rat data, lattice constants are 1.414nm and 1.483nm and distance between molecules are 1.00nm and 1.05nm respectively. As longer distance between molecules, charge transfer is hard and thermalization distance becomes smaller.

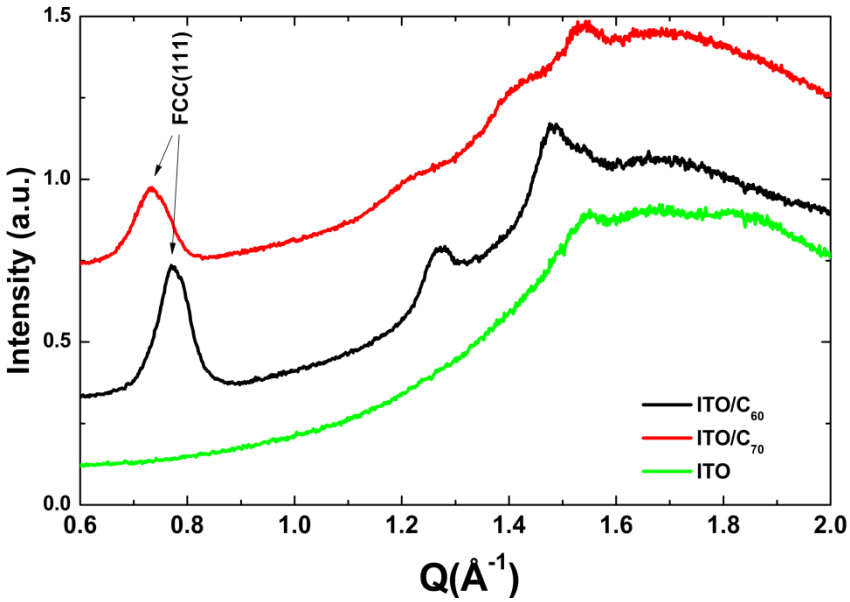

Figure 2.5 X-ray scattering data of C_{60} and C_{70} on ITO substrate.

2.4 Conclusion

In this chapter, photoconductivity of C_{60} and C_{70} is investigated. C_{70} has similar molecular structure and crystal structure. Both show photoconductivity and it is a function of exciton generation rate, internal electric field, and thermalization distance.

Absorption spectrum of C_{70} is different with that of C_{60}. Therefore overlap integral with solar spectrum is 2.3 times larger than that of C_{60} and photon absorption is 2.3 times larger. Accordingly, calculated exciton generation rate is 2.3 times larger than that of C_{60}. This is related with photoconductivity of C_{70} which is higher than that of C_{60}. But, increase in photoconductivity is only 1.7 times, due to difference in thermalization distance. Thermalization distance of C_{60} is longer than that of C_{70}; photon to electron conversion efficiency is different. It is confirmed with X-ray scattering data.

Chapter 3 Effect of work function of electrode

3.1 Introduction

Internal electric field in organic layer is affected by V_{app}, thickness of organic layer and V_{bi}. As shown in equation (1.4), bulk-ionization yield is a function of internal electric field. Therefore, not only applied voltage (V_{app}) but also V_{bi} affects photocurrent generated by bulk-ionization. To investigate effect of V_{bi}, work function of electrode is modified by inserting interfacial layer; here 5nm of MoO_3 and 1nm of ReO_3 are used as interfacial layer. When 5nm of MoO_3 and 1nm of ReO_3 are deposited on ITO substrates, work functions of electrode change to -6.8 eV and -6.0 eV. [15, 16] Accordingly, they change work function of electrode deeper. The V_{bi} are calculated by photoconductivity and measured by capacitance-voltage characteristics.

3.2 Experiments

Schottky solar cells has the following structure: indium tin oxide (ITO) (150 nm) / interfacial layer / C_{60} (60 nm) / BCP (8 nm) / AL (100 nm). 5 nm of MoO_3 and 1 nm of ReO_3 are used as interfacial layer.

The ITO-coated glass substrate was successively cleaned with acetone and isopropyl alcohol. The substrate was exposed to UV-O3 for 15 min before use. All the organic layers were deposited using thermal evaporation at the base pressure of ca. 10-7 torr with a rate of 1 Å/s without breaking the vacuum. MoO_3 and ReO_3 layers were also thermally deposited onto the substrate with a rate of 0.2 Å/s and 0.1 Å/s respectively. The devices had active areas of 2×2 mm^2. A patterned insulator on the ITO and the top cathode deposited through a shadow mask defined the cell area. After fabrication, the devices were encapsulated using the epoxy resin in N_2 environment. The photovoltaic properties of the device were measured with an AM 1.5G 100 mW/cm^2 solar simulator (300 W Oriel 69911A) light source and a source measurement unit (Keithley 237). The measurement set up was calibrated with a National Renewable Energy Laboratory-certified reference Si-solar cell covered with a KG-5 filter before every measurement.

3.3 Result and Discussion

Figure 3.1 shows J-V curves and IPCE spectra of fullerene based Schottky solar cells. In J-V curves, photocurrents of three devices increase linearly with increasing V_{app}. It means that photocurrent is generated by photoconductivity in fullerene bulk. Slope of J-V curves indicate field dependence of photoconductivity on V_{app} and large slope means that is large, in other word, bulk-ionization yield is high. At the same condition (same internal electrical field and same light intensity), more photocurrent is generated when bulk-ionization yield is high.

IPCE of C_{60} on ITO substrate shows different spectrum with other cases, from 550 to 600nm. Since intermolecular charge transfer exciton is generated in this region, extra peak in this region means C_{60} on ITO substrate forms higher aggregation than other two cases. It is analyzed by x-ray scattering. C_{60} on ITO substrate forms FCC(111), shown in Figure 4.2 in next chapter.

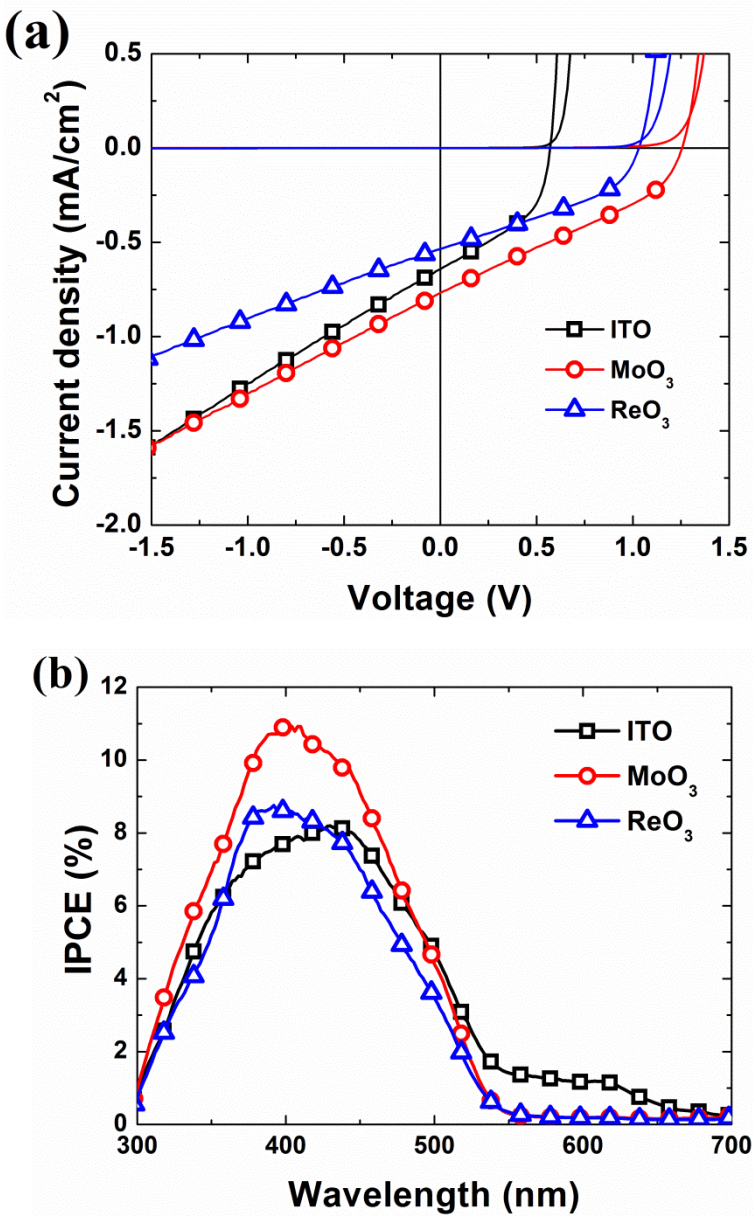

Figure 3.1 (a) J-V curves and (b) IPCE spectra of fullerene based Schottky solar cells

Table 3.1 The photovoltaic properties of fullerene based Schottky solar cells. Two interlayers are inserted between ITO and C_{60}.

Interface	PCE (%)	J_{SC} (mA/cm^2)	V_{OC}(V)	Fill Factor
ITO/C_{60}	0.17	0.64	0.57	0.44
MoO_3/C_{60}	0.31	0.77	1.24	0.33
ReO_3/C_{60}	0.21	0.54	1.03	0.38

.

Using equation (2.3), fittings of J-V curves of fullerene based Schottky solar cells are performed, shown in Figure 3.2.

Table 3.2 Fitted parameters from J-V curves.

Interface	J_S (mA/cm^2)	S (mA/cm^{2}V)	I (mA/cm^2)	n
ITO/C_{60}	8.68E-8	0.600	0.642	1.517
MoO_3/C_{60}	1.43E-11	0.500	0.783	2.178
ReO_3/C_{60}	1.79E-8	0.351	0.541	2.563

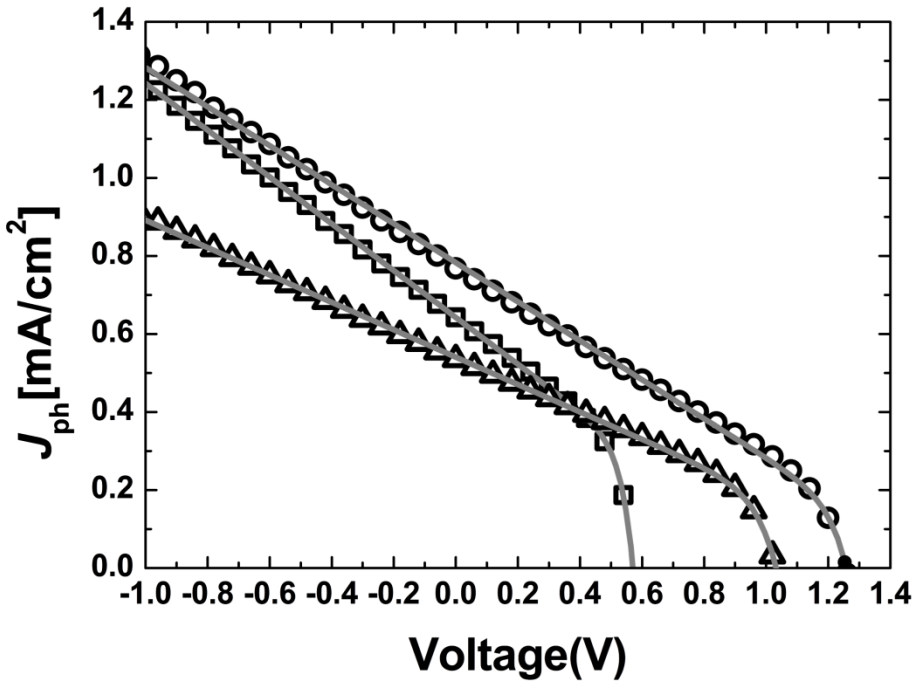

Figure 3.2 Fitting of J-V curves. Experimental results are represented by squares (ITO/C_{60}), circles (MoO_3/C_{60}), and triangles (ReO_3/C_{60}). The gray lines indicate fitted lines.

From the equation (2.6), thermalization distance and V_{bi} can be calculated with ε_r is 4.5 and T is 300 K.

$$r_0 = -\frac{r_c}{\ln\left(\frac{2kTd}{e^2 G r_c} S\right)} \tag{2.7}$$

$$V_{bi} = \frac{2kTd}{er_c}\left[-\frac{I}{eG}\exp\left(-\frac{r_c}{r_0}\right)-1\right] \tag{2.8}$$

Table 3.3 Calculated r_0 and V_{bi}.

Interface	r_0 (nm)	Cal. V_{bi} (V)
ITO/C_{60}	3.45	0.83
MoO_3/C_{60}	3.28	1.32
ReO_3/C_{60}	3.00	1.30

To compare Calculated V_{bi} with measured V_{bi}, capacitance-voltage characteristic is measured. When reverse voltage is applied to Schottky barrier, thickness of depletion layer goes thicker. When forward voltage is applied, thickness of that goes thinner. This means depletion width is a function of V_{app}, described as

$$W = \sqrt{\frac{2\varepsilon_r \varepsilon_0 (V_{bi} - V_{app})}{en}} \tag{2.9}$$

where e is element of charge, ε_r is the dielectric constant of material, ε_0 is

vacuum permittivity and *n* is carrier density. [13]

Charge carriers cannot pass the depletion width, and the depletion width acts like capacitance. Capacitance changes with depletion width; capacitance is also function of V_{app}, plotted in Figure 3.3.

$$C = \varepsilon_r \varepsilon_0 \frac{A}{W} = \varepsilon_r \varepsilon_0 A \sqrt{\frac{en}{2\varepsilon_r \varepsilon_0 (V_{bi} - V_{app})}} \tag{2.10}$$

With increasing V_{app}, depletion width decreases and at V_{bi}, depletion width disappears and current starts to flow. This condition, capacitance of device decreases rapidly. Changing band structure is shown in Figure 3.4.

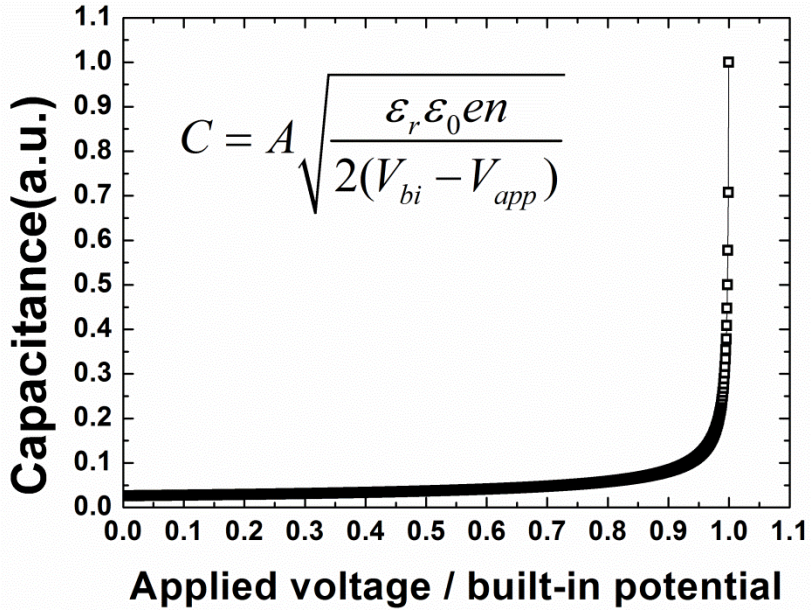

Figure 3.3 Change of capacitance with changing of V_{app}. Equation used here is inserted.

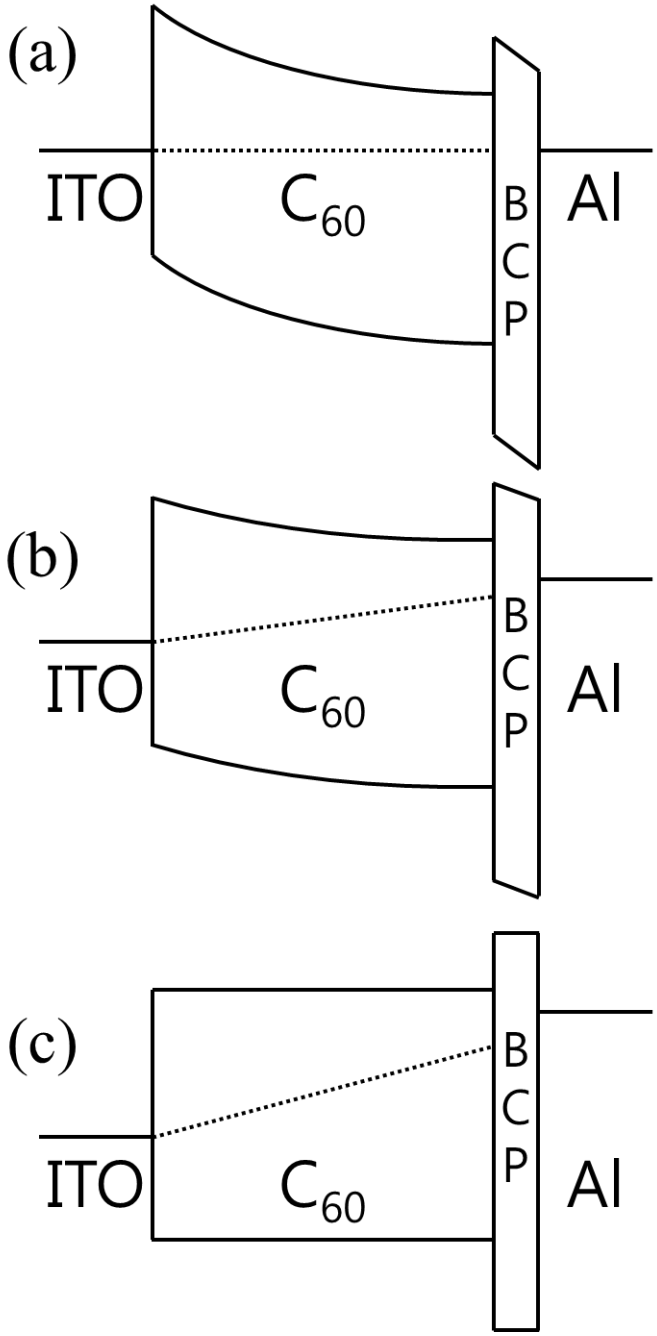

Figure 3.4 Band structures of fullerene based Schottky solar cells when applied voltages are (a) 0V, (b) 0.5 V_{bi}, (c) V_{bi}.

In Figure 3.5 (a), capacitance-voltage characteristic and J-V curve of dark condition are plotted for no interfacial layer device. Capacitance increases according to equation (2.10) and decreases rapidly at 0.78 V. This means that energy levels become flat band condition when V_{app} is 0.78 V. In other word, it is V_{bi}. It is same voltage where current starts to flow.

From measured V_{bi}, energy diagram can be drawn semi-quantitatively. Vacuum level shift (Δ) is calculated by the equation below;

$$\Delta = E_{F,\text{electrode}} - E_{F,C_{60}} - eV_{bi} \tag{2.11}$$

where E_F of ITO electrode is -4.8 eV and E_F of C_{60} is -4.5 eV. [17] Δ is calculated as 0.48 eV upward shown in Figure 3.5 (b).

Devices which contain MoO_3 and ReO_3 as interfacial layer are analyzed same method and shown in Figure 3.6 and 3.7 respectively. Then, measured V_{bi} and calculated V_{bi} are compared in Figure 3.8. Calculated V_{bi} of two devices are well matched with measured V_{bi}.

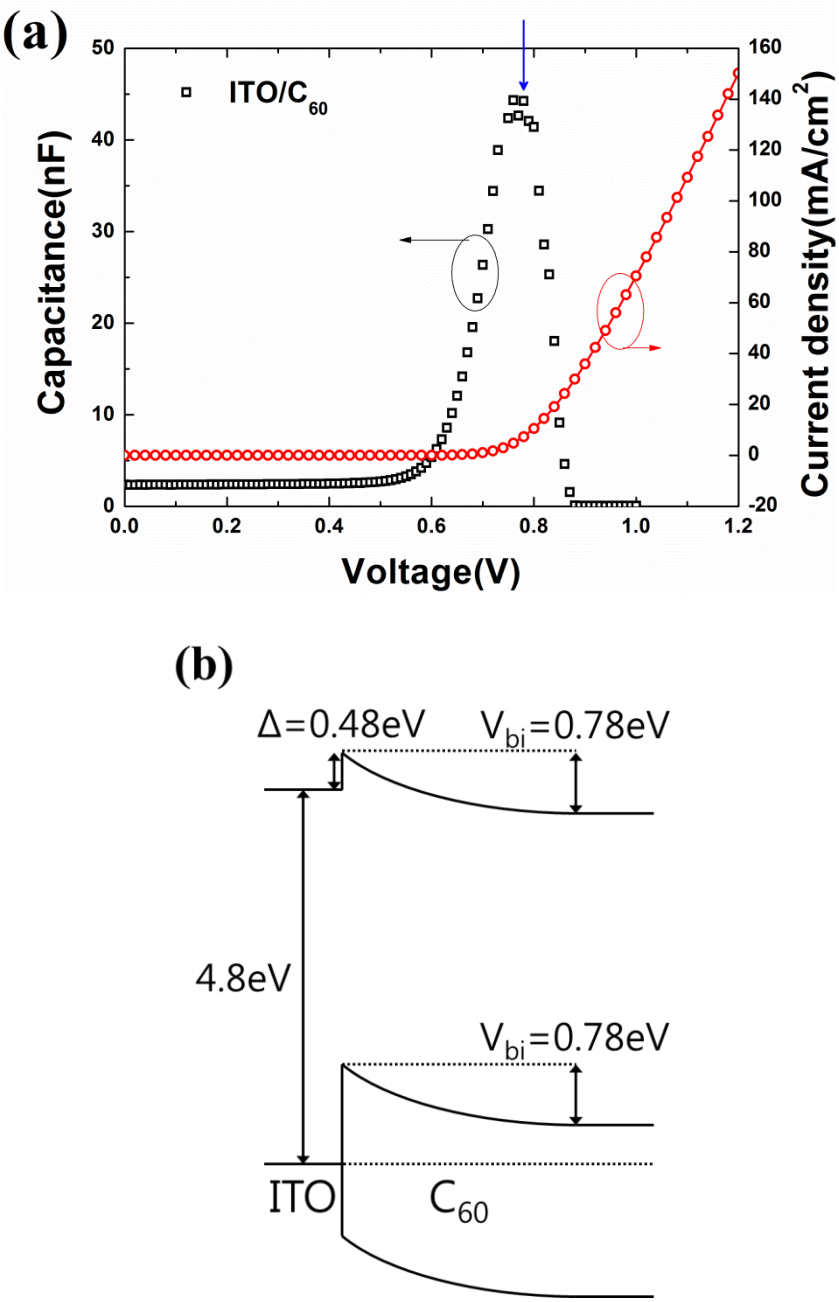

Figure 3.5 (a) C-V characteristic and dark current of device (b) energy band diagram of ITO/C_{60} contact.

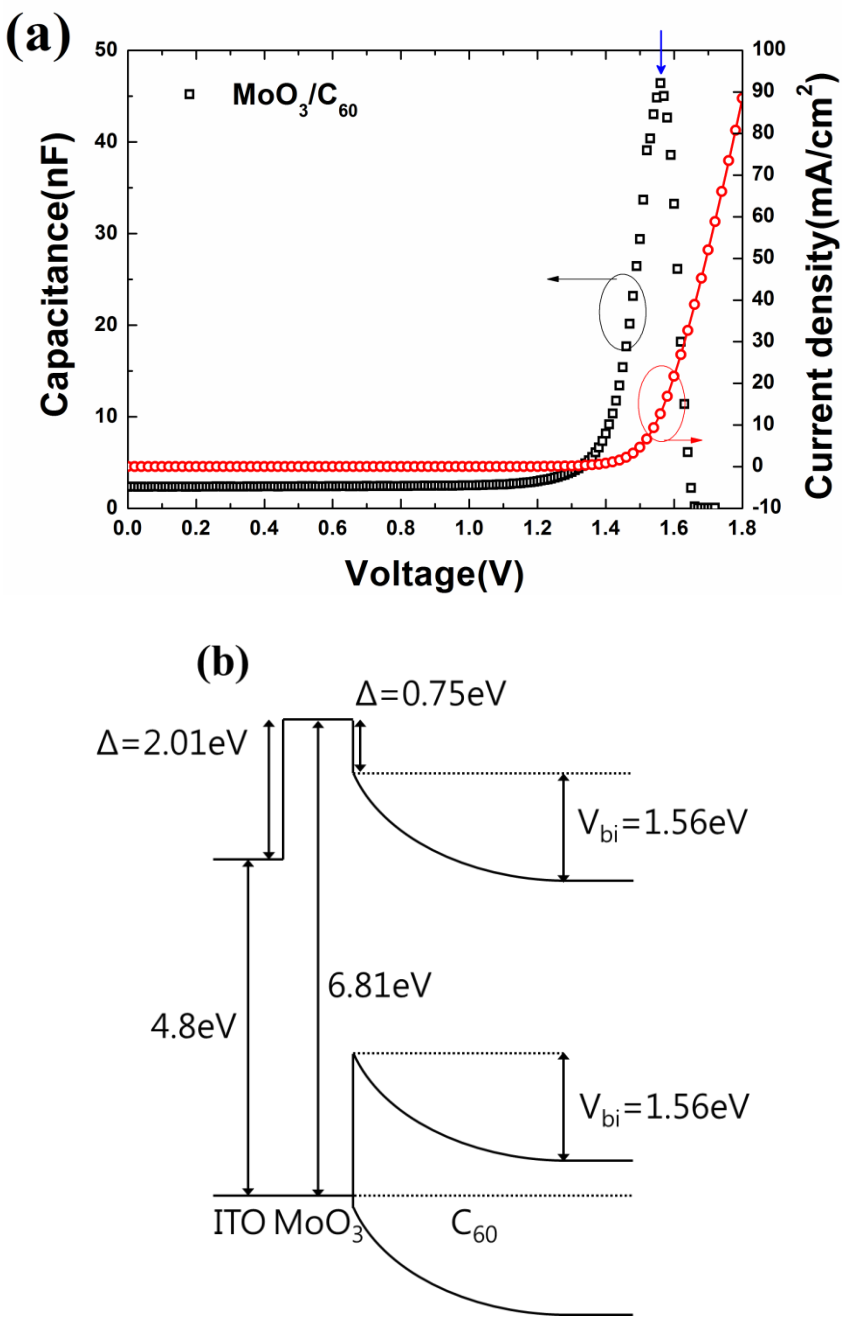

Figure 3.6 (a) C-V characteristic and dark current of device (b) energy band diagram of MoO_3/C_{60} contact.

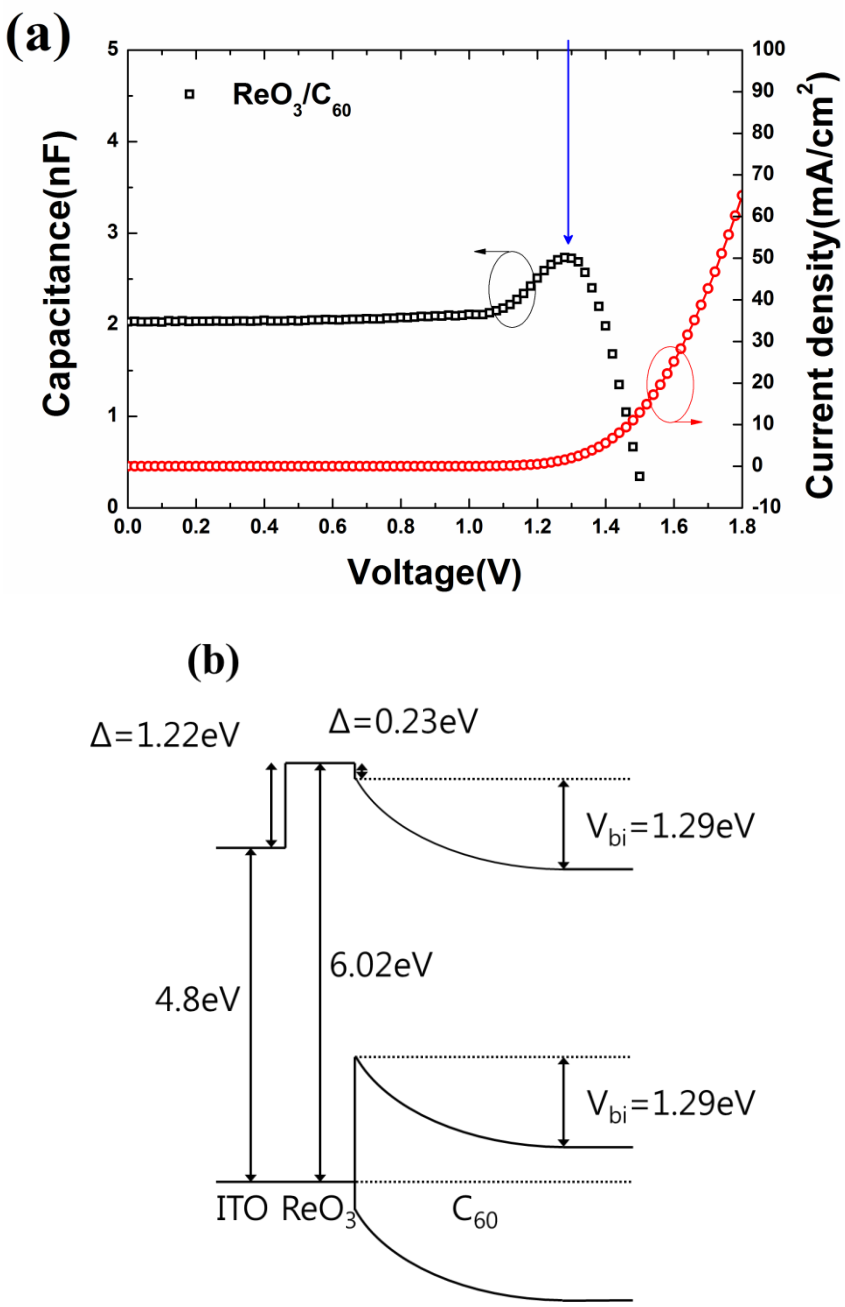

Figure 3.7 (a) C-V characteristic and dark current of device (b) energy band diagram of ReO_3/C_{60} contact.

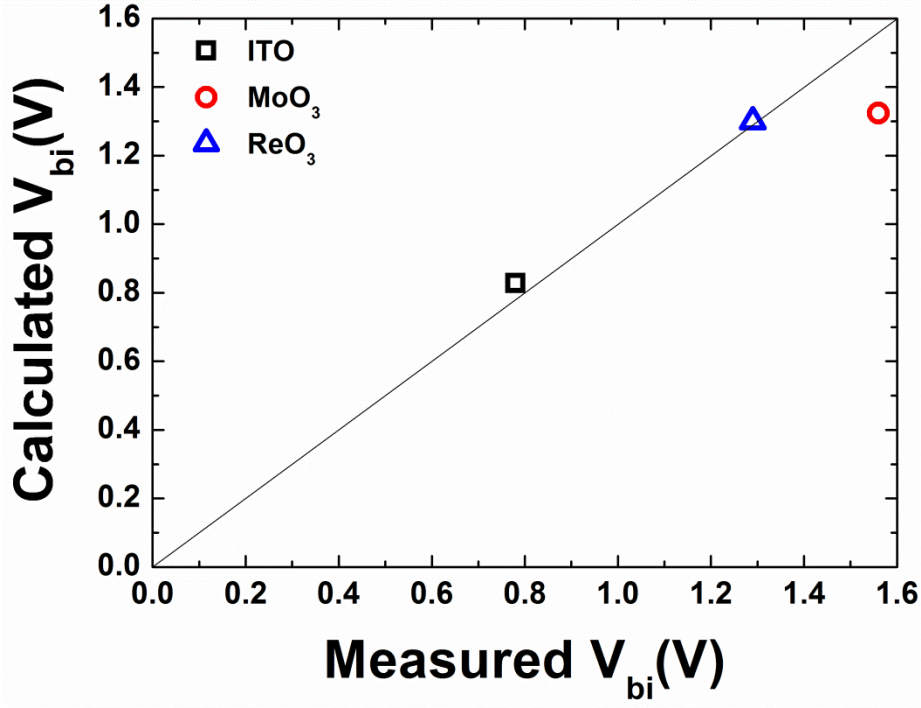

Figure 3.8 Comparison between calculated and measured V_{bi}. Solid line represents that calculated V_{bi} equals with measured V_{bi}.

3.4 Conclusion

The linear dependence of photocurrent in fullerene based Schottky solar cells is demonstrated. In the solar cells, the origin of photocurrent is bulk-ionization in fullerene. It is affected by internal electric field, a function of V_{bi} and V_{app}. V_{bi} is modified by changing work function of the electrode, with interfacial layer; MoO_3 and ReO_3. Inserting interfacial layer makes work function of electrode deeper, therefore V_{bi} increased. It is calculated with equation form photoconductivity and measured by C-V characteristics. Finally, band structure of interface can be drawn semi-quantatively.

Chapter 4 Effect of inserting CuI layer

4.1 Introduction

In this chapter, CuI layer is inserted as templating layer and effect of crystallinity on fullerene based Schottky solar cell is investigated. Crystallinity of fullerene is also factor that affects photoconductivity. Even though internal quantum efficiency is same, charge transport and collection can be affected by crystallinity. To investigate effect of crystallinity, CuI layer is inserted as templating layer CuI is known as templating layer for donor materials; however, effect of CuI on fullerene is not studied yet Here, the effects of inserting CuI layer are studied by UV-vis spectroscopy and GIWAXS.

4.2 Experiments

Schottky solar cells has the following structure: indium tin oxide (ITO) (150 nm) / interfacial layer / C_{60} (60 nm) / BCP (8 nm) / AL (100 nm). 5 nm of MoO_3 and 1 nm of ReO_3 are used as interfacial layer. Templating layer, 3 nm of CuI, is inserted between interfacial layer and C_{60} layer.

The ITO-coated glass substrate was successively cleaned with acetone and isopropyl alcohol. The substrate was exposed to UV-O3 for 15 min before use. All the organic layers were deposited using thermal evaporation at the base pressure of ca. 10-7 torr with a rate of 1 Å/s without breaking the vacuum. MoO_3, ReO_3, CuI layers were also thermally deposited onto the substrate with a rate of 0.2 Å/s, 0.1 Å/s, and 0.2 Å/s respectively. The devices had active areas of 2×2 mm^2. A patterned insulator on the ITO and the top cathode deposited through a shadow mask defined the cell area. After fabrication, the devices were encapsulated using the epoxy resin in N_2 environment. The photovoltaic properties of the device were measured with an AM 1.5G 100 mW/cm^2 solar simulator (300 W Oriel 69911A) light source and a source measurement unit (Keithley 237). The measurement set up was calibrated with a National Renewable Energy Laboratory-certified reference Si-solar cell covered with a KG-5 filter before every measurement. The UV-Vis absorption spectra of films were recorded with a VARIAN Cary 5000 UV-vis spectrophotometer. The crystalline properties were investigated by synchrotron x-ray scattering measurements at 5A x-ray scattering beamline for materials science of Pohang Light Source II (PLS-II). The x-ray wavelength was 1.071 Å (11.58 keV). The films were deposited on ITO substrates.

4.3 Result and Discussion

In this chapter, CuI layer is inserted as templating layer and effect of crystallinity on fullerene based Schottky solar cell is investigated. CuI is known as templating layer for donor materials; however, effect of CuI on fullerene is not studied yet.

First, effect of CuI on crystallinity is investigated by UV-vis spectroscopy. In Figure 4.1, absorbance of intermolecular interaction peak around 400 to 600nm is increased. Even though absorbance of CuI layer is negligible, absorbance of C_{60} film is increased and this means that CuI layer act as templating layer. However, since the increase of crystallinity is not shown clearly in absorbance, x-ray experiment is performed additionally.

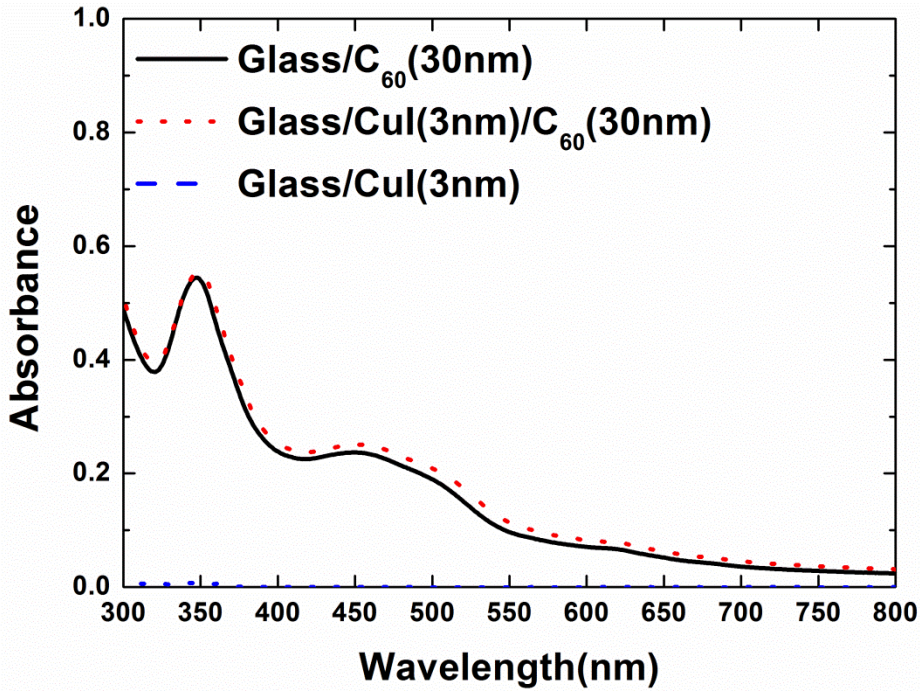

Figure 4.1 Absorption spectra of organic films. Solid line, dotted line and dashed line represent C_{60} on class, C_{60} on CuI and CuI on glass, respectively.

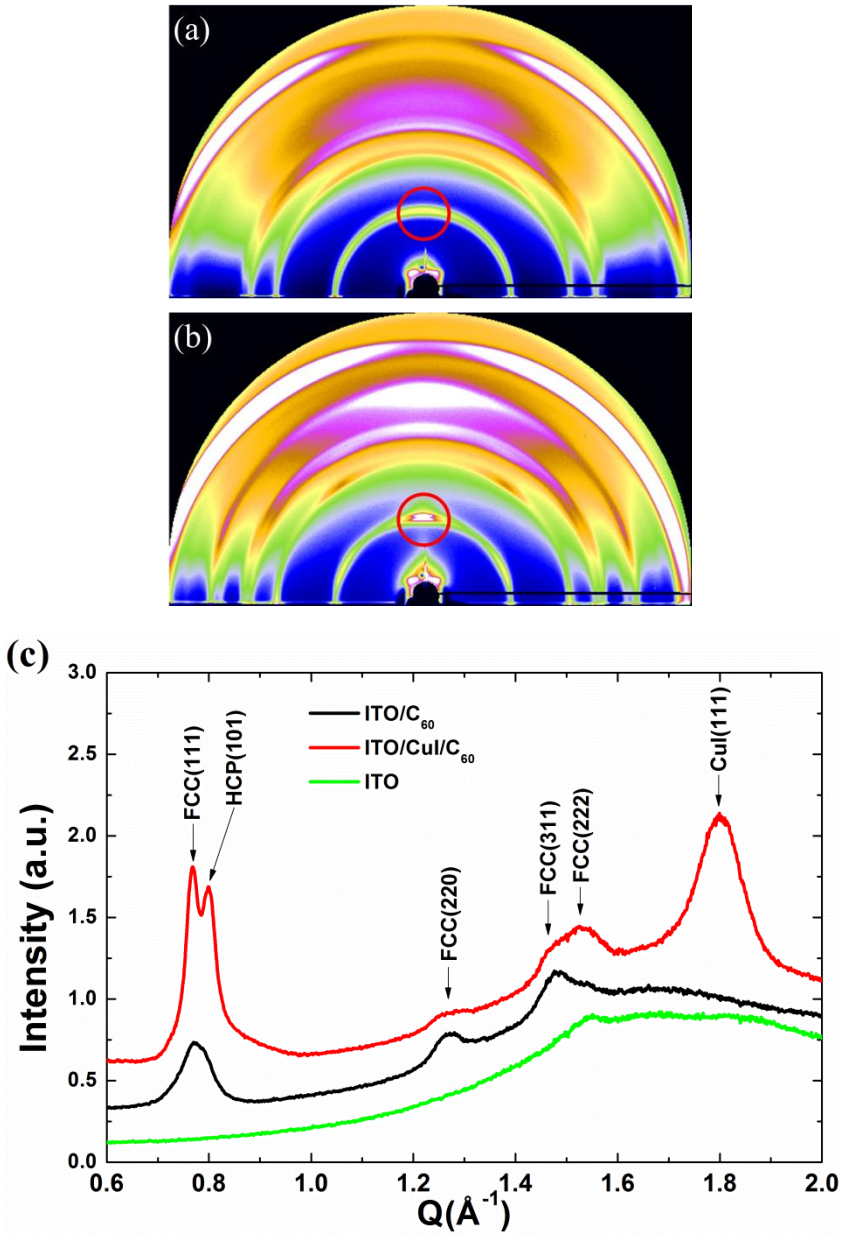

Figure 4.2 GIWXAS images of (a) 60nm of C_{60} on ITO and (b) 60nm of C_{60} on ITO with 3nm of CuI layer between them. (c) Vertical cuts of GIWAXS images.

Usually, x-ray experiment was performed on silicon substrate, to get clear signal. However, structures of organic layers grown on silicon substrates are different with those of organic layers grown on ITO substrate. Here, x-ray experiment is performed on ITO substrate to make same condition with device for C_{60} crystal.

In figure 4.2, GIWAXS images of C_{60} are shown. The images indicate that crystallinity of C_{60} is increased when 3nm of CuI layer is inserted. It is clearly shown in vertical cuts of GIWAXS images, in Figure 4.2 (c).

In Figure 4.2 (c), C_{60} on ITO substrate shows peaks at Q = 0.77 $Å^{-1}$, Q = 1.27 $Å^{-1}$and Q = 1.46 $Å^{-1}$ which assigned as the (111) plane of the face-centered cubic (FCC) of C_{60}, (220) plane of the FCC of C_{60} and (311) plane of the FCC of C_{60}. [18-20] It is saying that C_{60} on ITO forms FCC crystal structure leading to extra aggregation peak (in Figure 3.1).

Otherwise, C_{60} on 3nm of CuI layer deposited on ITO surface shows differences compare to case of C_{60} on ITO. In this case, three peaks are added at Q = 0.80 $Å^{-1}$, Q = 1.53 $Å^{-1}$and Q = 1.80 $Å^{-1}$ which assigned as the (101) plane of the hexagonal crystal packing (HCP) of C_{60}, (222) plane of the FCC of C_{60} and (111) plane of zinc blende structure of CuI. [21]

Here, peak of FCC(111) increased. Peak of HCP(101) which implies stacking fault of FCC(111) and peak of FCC(222) are developed too. [18-20] But peaks of FCC(220) and FCC(311) are declined. As distance between two adjacent and parallel planes is the shortest in FCC(111), mobility of [111] direction is fastest. Here, inserting CuI layer induces FCC(111) plane parallel to substrate and this makes mobility of vertical direction to substrate increase.

To investigate CuI effect on devices, 3nm of CuI layer is inserted in three devices analyzed above. However, effect of inserting CuI layer between ITO

and C_{60} on bulk-ionization yield is negligible, only 2.5% increase in slope of J-V curves is observed. This indicates that crystallinity of C_{60} on ITO substrate is enough to charge transport and charge collection. In other word, the effect of increase in crystallinity of C_{60} by inserting CuI layer on charge transport and collection is negligible. Only V_{OC} is increased significantly due to large work function of CuI, which is -5.4 eV form vacuum level. [22]

In Figure 4.3 (a) and (b), J-V curves and IPCE spectra of these two devices are shown respectively. As explained above, slope of J-V curves are similar to each other. Moreover, both structure show aggregation peak from 550 to 600nm, meaning intermolecular interaction between C_{60} molecules.

Table 4.1 The photovoltaic properties of fullerene based Schottky solar cells. CuI layer is inserted as templating layer.

Interface	PCE (%)	J_{SC} (mA/cm^2)	V_{OC} (V)	Fill Factor
ITO/C_{60}	0.17	0.64	0.57	0.44
ITO/CuI/C_{60}	0.23	0.72	0.89	0.36

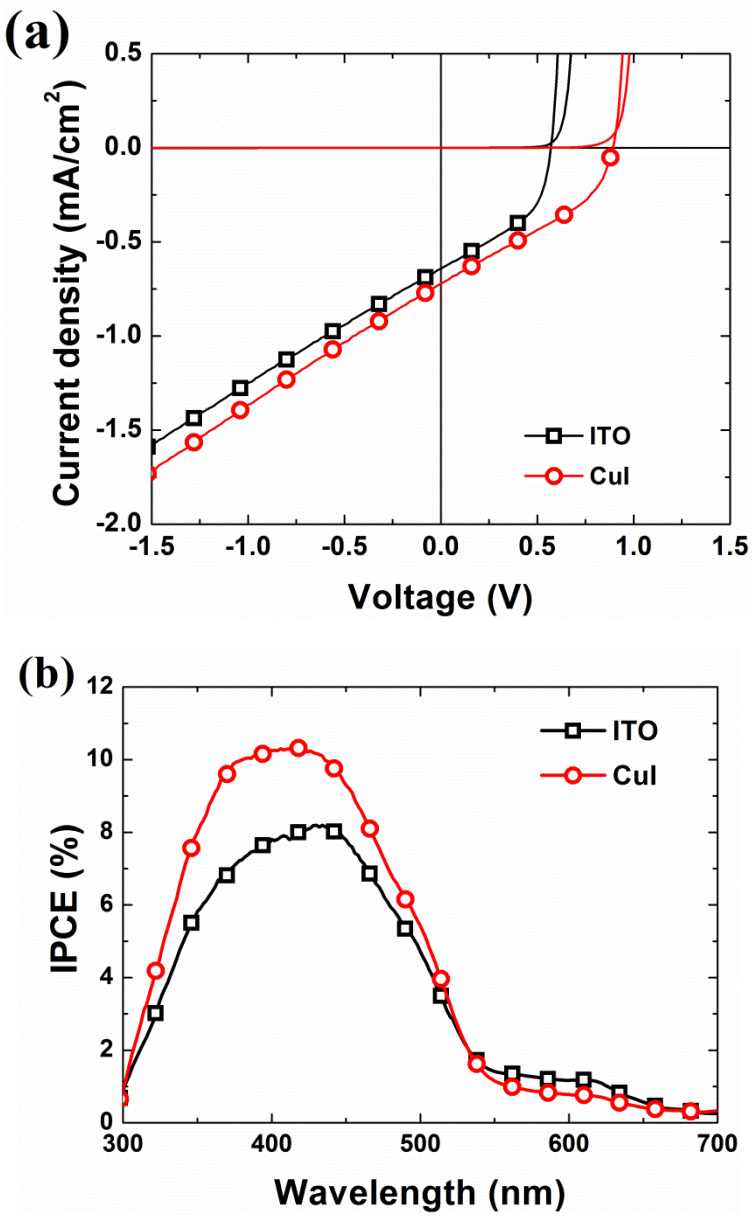

Figure 4.3 (a) J-V curves and (b) IPCE spectra of fullerene based Schottky solar cells. CuI layer is inserted.

In case of MoO_3 is used as interfacial layer, effect of inserting CuI layer is significant. As shown in Figure 3.1 (a) and (b), 5nm of MoO_3 layer deposited on ITO substrate interrupts C_{60} to form aggregation. It is interpreted by slope of J-V curves and IPCE spectra. As explained above, increase in slope of J-V curve means large bulk-ionization yield.

Here, inserting 3nm of CuI layer induces C_{60} to form aggregation, as shown in Figure 4.4. Slope of J-V curve is increased 43.8% and peak at 550~600nm is observed when 3nm of CuI layer is inserted. This result is supported by x-ray experiment, Figure 4.2.

However, in case of MoO_3/CuI/C_{60} interface, photocurrent is increased rapidly at 0.8V and dark current injection starts at 1.1V. This difference makes remarkable decrease in V_{OC}, which is decreased 0.43 V compared to MoO_3/ C_{60} interface.

ReO_3 used case shows similar result with previous MoO_3 case in IPCE spectra in Figure 4.5 (b). However, in Figure 4.5 (a), there is interesting result in J-V curves. Slope of J-V curve increased 93.5%, with double value of MoO_3 case, and decrease in V_{OC} is only 0.09V which is five times smaller than MoO_3 case. Using this result, high efficiency solar cells up to 6% is achieved, discussed in next chapter.

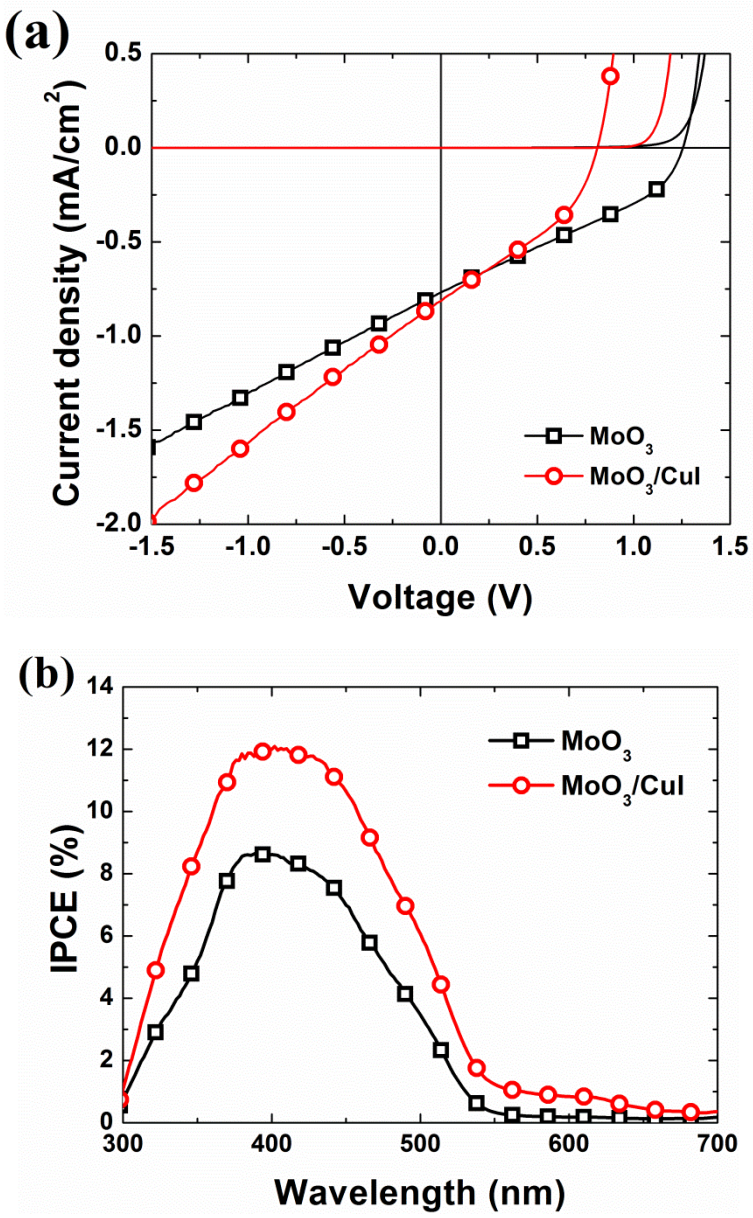

Figure 4.4 (a) J-V curves and (b) IPCE spectra of fullerene based Schottky solar cells in case of MoO_3 used. CuI layer is inserted.

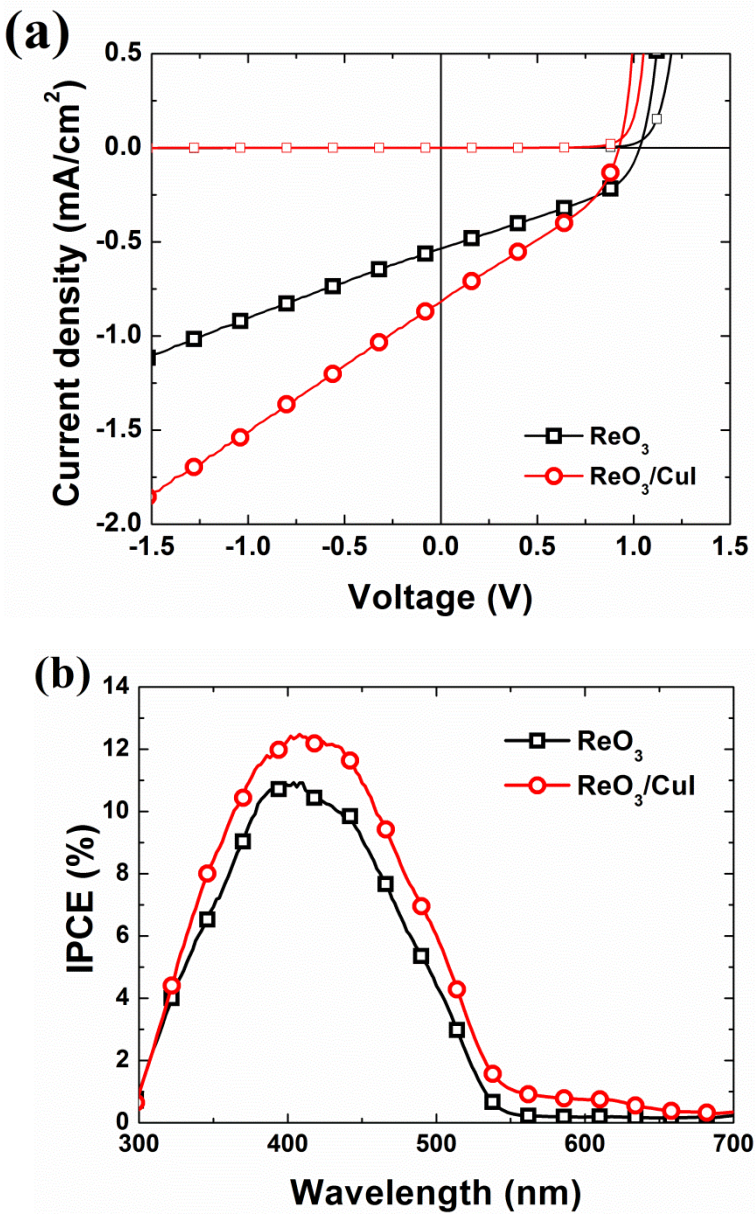

Figure 4.5 (a) J-V curves and (b) IPCE spectra of fullerene based Schottky solar cells in case of ReO_3 used. CuI layer is inserted.

Table 4.2 The photovoltaic properties of fullerene based Schottky solar cells. CuI layer is inserted as templating layer in two cases, MoO_3 used and ReO_3 used case.

Interface	PCE (%)	J_{SC} (mA/cm^2)	V_{OC} (V)	Fill Factor
MoO_3/C_{60}	0.31	0.77	1.24	0.33
$MoO_3/CuI/C_{60}$	0.24	0.81	0.81	0.37
ReO_3/C_{60}	0.21	0.54	1.03	0.38
$ReO_3/CuI/C_{60}$	0.26	0.82	0.94	0.33

Using equation (2.3), fittings of J-V curves of fullerene based Schottky solar cells are performed, shown in Figure 4.6. Then, parameters from fittings and equation (2.7), (2.8) lead thermalization distance and V_{bi}, as summarized in Table 4.3.

Table 4.3 Fitted and calculated parameters from J-V curves.

Interface	J_S (mA/cm^2)	S (mA/cm^{2}V)	I (mA/cm^2)	n	r_0 (nm)	Cal. V_{bi} (V)
$ITO/CuI/C_{60}$	1.21E-12	0.615	0.733	1.393	3.47	0.95
$MoO_3/CuI/C_{60}$	4.84E-6	0.719	0.824	3.016	3.63	0.90
$ReO_3/CuI/C_{60}$	2.75E-9	0.679	0.821	2.056	3.57	0.97

To compare calculated V_{bi} with measured V_{bi}, capacitance-voltage characteristic is measured as shown Figure 4.7 and summarized in Table 4.4.

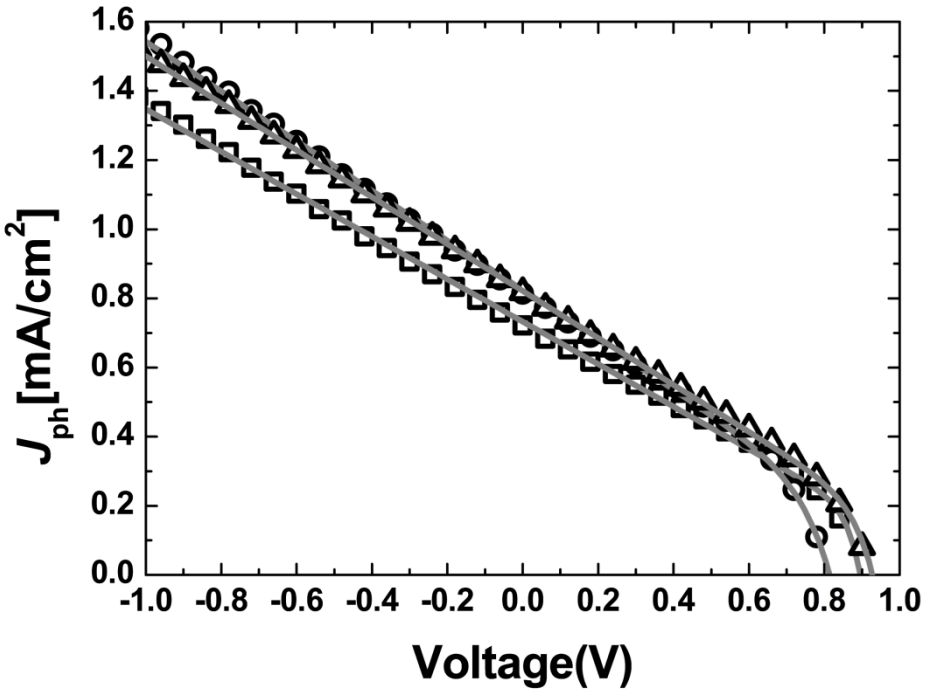

Figure 4.6 Fitting of J-V curves. Experimental results are represented by squares (ITO/CuI/C_{60}), circles (MoO_3/CuI/C_{60}), and triangles (ReO_3/CuI/C_{60}). The gray lines indicate fitted lines.

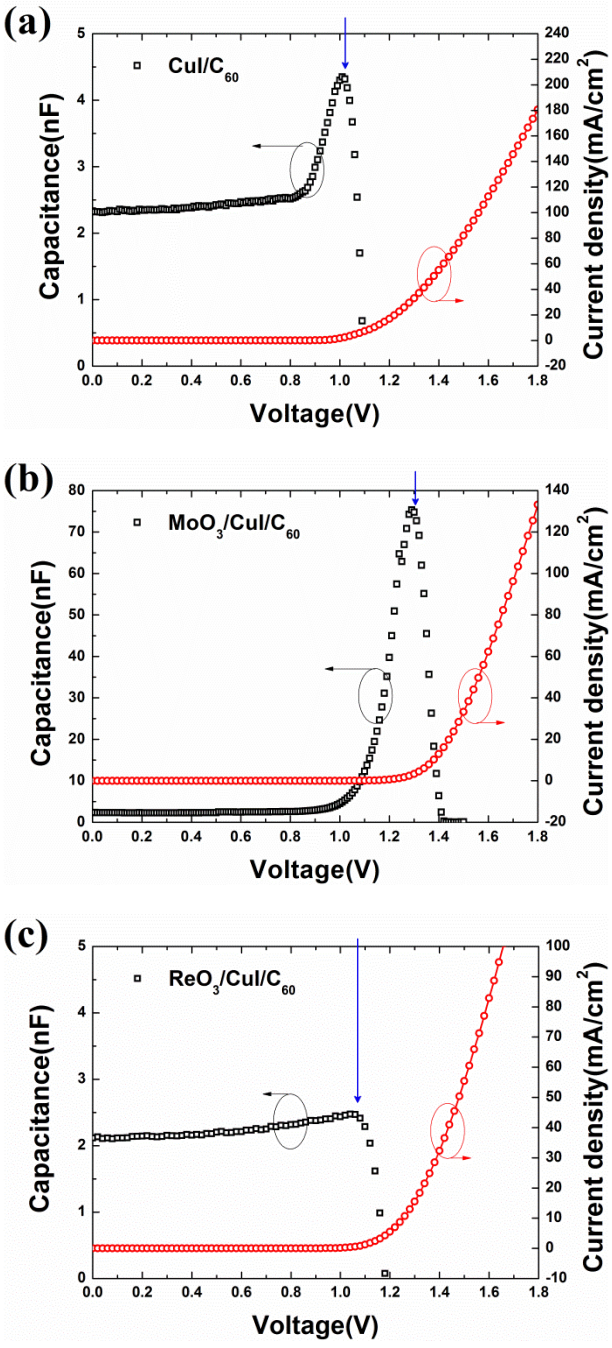

Figure 4.7 C-V characteristics and dark currents of devices of (a) CuI (b) MoO_3/CuI (c) ReO_3/CuI used.

Table 4.4 Summarization of fitted and calculated parameters from J-V curves

Interface	V_{OC} (V)	V_{bi} (V)	S (mA/cm^2V)	I (mA/cm^2)	r_0 (nm)	Cal. V_{bi} (V)
ITO/C_{60}	0.57	0.78	0.600	0.642	3.45	0.83
ITO/CuI/C_{60}	0.89	1.02	0.615	0.733	3.47	0.95
MoO_3/C_{60}	1.24	1.56	0.500	0.783	3.28	1.32
MoO_3/CuI/C_{60}	0.81	1.31	0.719	0.824	3.63	0.90
ReO_3/C_{60}	1.03	1.29	0.351	0.541	3.00	1.30
ReO_3/CuI/C_{60}	0.94	1.07	0.679	0.821	3.57	0.97

As shown in Figure 4.7, capacitance increases according to equation (2.10) and decreases rapidly at V_{bi} where current injection is started. Here, calculated V_{bi} and measured V_{bi} are compared in Figure 4.8. Except for MoO_3 used devices, calculated V_{bi} of all devices are well matched with measured V_{bi}.

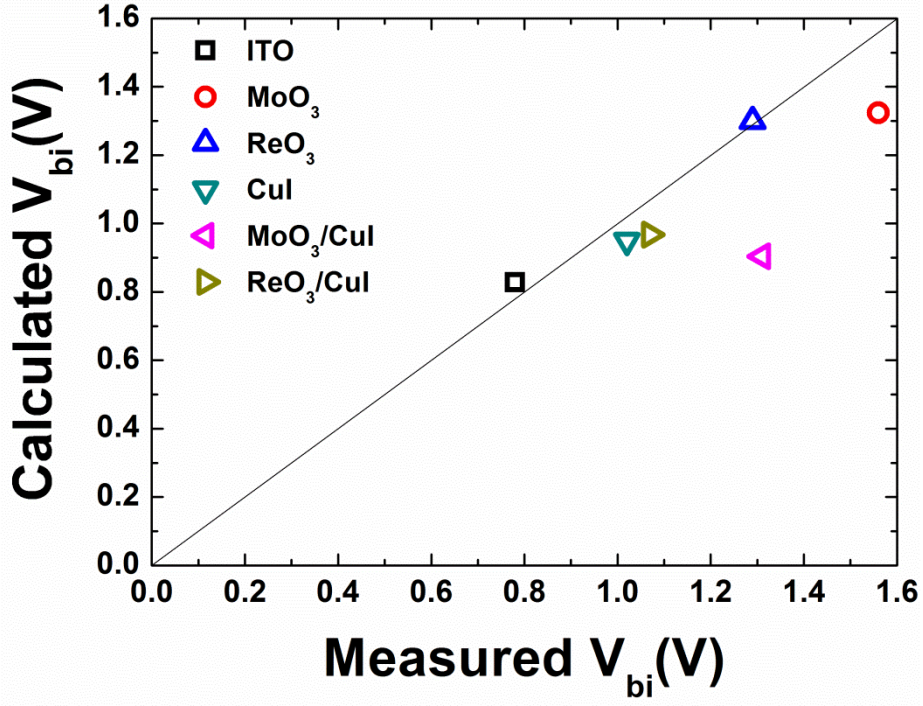

Figure 4.8 Comparison between calculated and measured V_{bi}. Solid line represents cal. V_{bi} = mea. V_{bi}.

4.4 Conclusion

In this chapter, CuI layer is inserted as templating layer and effect of crystallinity on fullerene based Schottky solar cell is investigated. Increase in crystallinity is clearly observed in GIWAXS and crystal structures are ordered to FCC(111). This means mobility of vertical direction to substrate is increased. It is shown in J-V curves. Especially, device which has ReO_3/CuI interface shows impressive increase (93.5%) in photoconductivity. Moreover, in this case, decrease of V_{OC} is much smaller than that of MoO_3 case. This result leads high efficiency solar cells, discussed next chapter.

Chapter 5 Low-donor concentration solar cells

5.1 Introduction

Recently, high efficiency solar cells (>5%) with low donor concentration are reported. [23- 26] It consists of large portion of fullerene, and small portion of donor materials with Schottky barrier between fullerene bulk and high work function electrode. Up to now, effect of change donor materials and concentration are reported. [27, 28] However, in this chapter, interfacial layer between ITO electrode and fullerene based photo-active layer is investigated.

In previous chapter, effects of changing interfacial layers on fullerene based Schottky solar cells are studied. Since low-donor concentration solar cells include fullerene based Schottky barrier, research discussed in previous chapter can be applied to low-donor concentration solar cells. Therefore, in this chapter, interfacial layer as which MoO_3 is usually used is modified and device characteristics are measured.

5.2 Experiments

Low-donor concentration solar cells have the following structure: indium tin oxide (ITO) (150nm) / interfacial layer / C_{70}: TAPC 5 vol% (60nm) / BCP (8nm) / AL (100nm). 5nm of MoO_3 and 1nm of ReO_3 are used as interfacial layer. Templating layer, 1nm of CuI, is inserted between interfacial layer and doped C_{60} layer, shown in Figure 5.1.

The ITO-coated glass substrate was successively cleaned with acetone and isopropyl alcohol. The substrate was exposed to UV-O3 for 15 min before use. All the organic layers were deposited using thermal evaporation at the base pressure of 7×10^{-7} torr without breaking the vacuum. Deposition rate of active layer was 2 Å/s, with 1.95 Å/s of C_{70} and 0.05 Å/s of TAPC. BCP and Al were deposited with rate of 1 Å/s and 4 Å/s respectively. MoO_3, ReO_3, CuI layers were also thermally deposited onto the substrate with a rat of 0.2 Å/s, 0.1 Å/s, and 0.2 Å/s respectively. The devices had active areas of 2×2 mm^2. A patterned insulator on the ITO and the top cathode deposited through a shadow mask defined the cell area. After fabrication, the devices were encapsulated using the epoxy resin in N_2 environment. The photovoltaic properties of the device were measured with an AM 1.5G 100 mW/cm^2 solar simulator (300 W Oriel 69911A) light source and a source measurement unit (Keithley 237). The measurement set up was calibrated with a National Renewable Energy Laboratory-certified reference Si-solar cell covered with a KG-5 filter before every measurement.

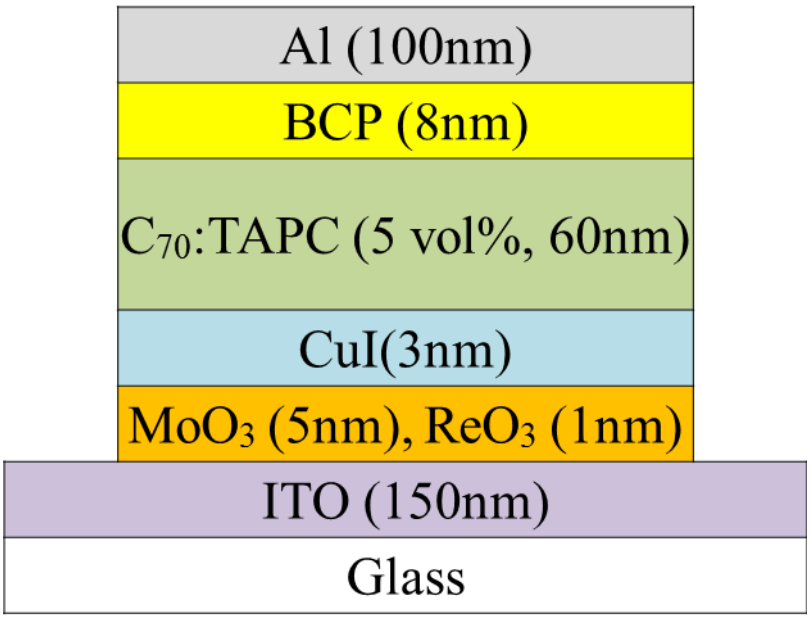

Figure 5.1 Device structure of low-donor concentration solar cells.

5.3 Result and Discussion

Four devices are fabricated and J-V characteristics of them are measured, summarized in Table 5.1 and shown in Figure 5.2.

In 60nm pure of C_{70} layer, photon absorption rate is 7.444×10^{16} /cm^2·s, which is calculated by transfer matrix method. If all of these photons are changed to charge carriers and the collection efficiency is 100%, the value of current density should be 11.93mA/cm^2. As shown in Table 5.1, values of J_{SC} in 4 devices are closed to the ideal current density, with error range of only 2%. This means that photocarriers in active layer are collected almost 100% at short-circuit condition.

Changes in V_{OC} of 4 devices are similar with previous results, shown in Table 4.2 and 3.1. V_{OC} of MoO_3 used and ReO_3 used device show same values, however, when CuI layer is inserted, V_{OC} of two devices are decreased. In MoO_3 used case, V_{OC} decreased 0.04 V, which is 4times larger than ReO_3 case. Only decrease of 0.01 V is observed in ReO_3 used case.

Changes in fill factors are due to increase of crystallinity. In Figure 4.2, it is observed that CuI induces FCC(111) of C_{60} and C_{70} has very similar structure with C_{60}. Here, this effect is shown in Fill factors in both cases, with increase in fill factors. In fullerene based Schottky solar cells, slopes of J-V curves are main parameter in photoconductivity, but in low-donor concentration solar cells, fill factors are main parameter because changes in J_{SC} are negligible and decreases in V_{OC} are small. When CuI layer is inserted between MoO_3 and fullerene matrix, PCE is small increased although V_{OC} is decreased. This is due to increase in crystallinity of C_{70}. On the other hand, inserting CuI layer between ReO_3 and fullerene matrix makes remarkable increase, value of

20.8%. Also PCE of devise is increased, value of 20.0%, and high efficiency solar cell up to 6% is achieved.

Table 5.1 The photovoltaic properties low-donor concentration solar cells.

Interfacial layer	PCE (%)	J_{SC} (mA/cm^2)	V_{OC} (V)	Fill Factor
MoO_3	5.51±0.02	11.65±0.09	0.91±0.02	0.52±0.01
MoO_3/CuI	5.57±0.01	11.60±0.06	0.87±0.00	0.55±0.00
ReO_3	5.16±0.04	11.78±0.04	0.91±0.01	0.48±0.00
ReO_3/CuI	6.19±0.07	11.85±0.12	0.90±0.01	0.58±0.01

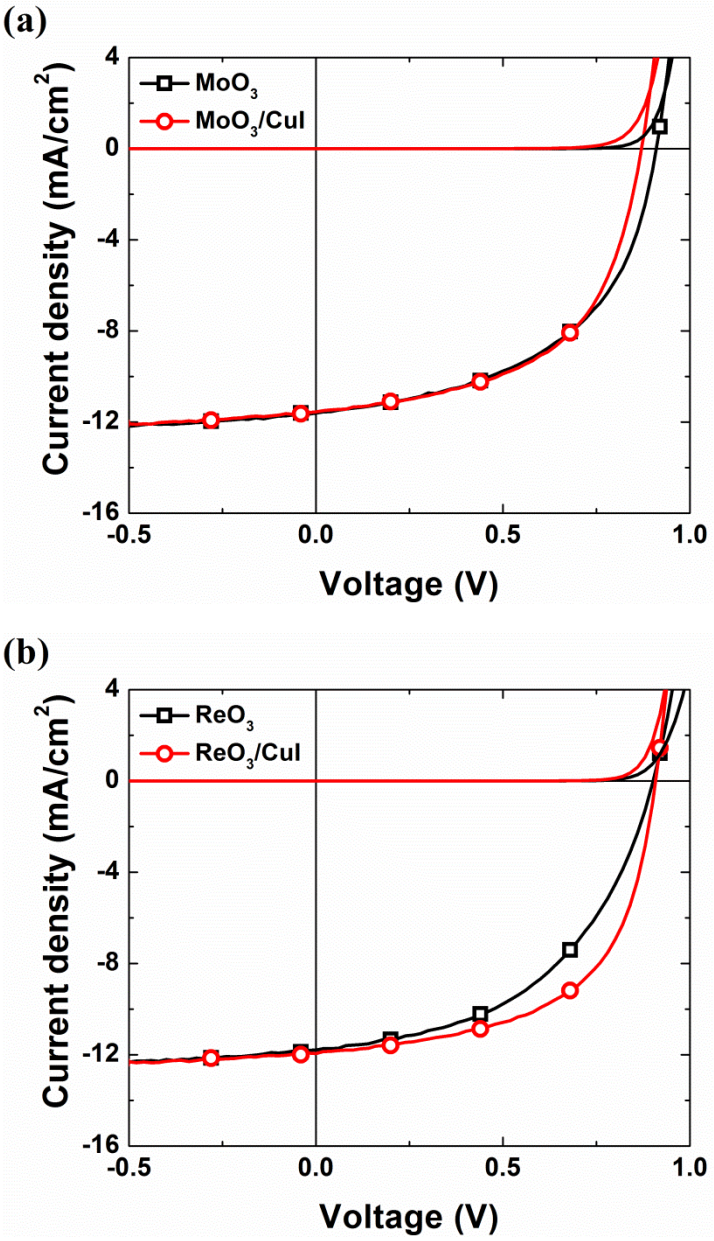

Figure 5.2 J-V curves of (a) MoO_3 used and (b) ReO_3 used low-donor concentration solar cells

5.4 Conclusion

In this chapter, interfacial layers of low-donor concentration solar cells are modified and the effects of that have been investigated by J-V characteristic under AM 1.5G 100 mW/cm^2. J_{SC} which is generated from photon absorption is closed to ideal current density in all cases. It indicates that charge collection efficiency is almost 100% in short-circuit condition. Changes of V_{OC} show similar result with fullerene based solar cells because Schottky barriers are main factors of determining V_{OC}. When CuI layer is inserted, fill factors are increased in both cases, due to the increase in crystallinity. Especially, ReO_3 used device shows remarkable increase of fill factor about 20.8%, leading increase of PCE about 20.0% and high efficiency solar cells with 6.2% are achieved. Using other materials, e.g. DIBSQ or DBP which show PCE over the 6% in reference devices, over the 7% will be achievable.

Summary

In this thesis, C_{60} based Schottky solar cells are fabricated and analyzed by J-V characteristics, IPCE spectra, C-V characteristics and GIWAXS. Then, low-donor concentration solar cells are fabricated and analyzed by J-V characteristics.

Since fullerene has intrinsic charge carriers, band bending occurs in fullerene layer and Schottky barrier is formed with internal electric field. This field forces excitons to dissociate in fullerene matrix. Solar cells that contain this barrier are called Schottky solar cells.

C_{70}, one of the fullerene derivatives, shows photoconductivity like C_{60}. As overlap integral with solar spectrum of C_{70} is larger, photoconductivity of C_{70} is larger than C_{60}. But photon to electron conversion efficiency of C_{60} is larger than C_{70} because of difference in thermalization distance. It is calculated with equation from photoconductivity and discussed with X-ray scattering date.

In fullerene based Schottky solar cells, V_{bi} is changed with different interfacial layers. To obtain the V_{bi}, calculation and C-V measurement are performed. In C-V characteristics, voltage where capacitance decreases rapidly is same with the one where current starts to flow, defined as V_{bi}. Except for MoO_3 used devices, this is well matched with calculated $V_{bi.}$

C_{60} on CuI layer shows higher crystallinity than C_{60} on ITO. On the ITO substrate, C_{60} forms FCC(111) plane and when CuI layer is inserted between them, peak of FCC(111) is increased remarkably in GIWAXS images. This result is observed in device data. When CuI layer is inserted between electrode and active layer, photoconductivity is increased 43.8% in MoO_3 used device and 93.5% in ReO_3 used device.

With effect of CuI, low-donor concentration solar cells are modified. In MoO_3 used devices, increase in PCE is negligible due to decrease in V_{OC}, however, remarkable enhancement is observed in ReO_3 used devices. Here, maximized PCE is 6.2%.

References

[1] R. Pandey, A. A. Gunawan, K. A. Mkhoyan, R. J. Holmes, *Adv. Funct. Mater.* **2011**, 22, 617.

[2] S. Braun, W. R. Salaneck, M. Fahlman, *Adv. Mater.* **2009**, 21, 1

[3] M. Pope, C. E. Swenberg, in *Electronic Processes in Organic Crystals and Polymers*, 2nd ed., Oxford University Press , New York **1999**

[4] W. -I. Jeong, Y. E. Lee, H. -S. Shim, T. -M. Kim, S. -Y Kim, J. -J Kim, *Adv. Funct. Mater.* **2012**, 22, 3089

[5] H. -S. Shim, H. J. Kim, J. W. Kim, S. -Y Kim, W. -I. Jeong, T. -M. Kim, J. -J Kim, *J. Mater. Chem.* **2012**, 22, 9077

[6] J. W. Kim, H. J. Kim, T. -M. Kim, T. F. Kim, F. -H Lee, J. W. Kim, J. -J. Kim, *Curr. Appl. Phys.* **2013**, 7

[7] C. H. Cheng, J. Wang, G. T. Du, S. H. Shi, Z. J. Du, Z. Q. Fan, J. M. Bian, M. S. Wang, *Appl. Phys. Lett.* **2010**, 97, 083305

[8] A. Moliton, J. -M Nunzi, *Polym. Int.* **2006**, 55, 583

[9] L. Onsager , *Phys. Rev.* **1938** , 54 , 554

[10] R. E. Hummel, in *Electronic Properties of Materials*, 3rd ed., Springer Press , **2001**.

[11] K. Kudo, T. Saraya, S. Kuniyoshi, K. Tanaka, *Mol. Cryst. Liq. Cryst.* **1995**, 267, 423

[12] B. Yang, F. Guo, Y. Yuan, Z. Xiao, Y. Lu, Q. Dong, J. Huang, *Adv. Mater.* **2013**, 25, 572

[13] S. M. Sze, K. K. Ng, in *PHYCS OF SEMICONDUCTOR DEVECES*, 3rd ed., Wiley-Interscience Press , **2007**

[14] . L. A. A. Pettersson, L. S. Roman, O. Inganas, *J. Appl. Phys.* **1999**, 86, 487

[15] Y. Zhao, J. Chen, W. Chen, D. Ma, *J. APpl Phys.* **2012**, 111, 043716

[16] I. D. Baikie, U. Peterman, B. Lagel, K. Dirscherl, *J. Vac. Sci. Technol. A* **2001**, 19, 1460

[17] S Lee, J. –H. Lee, J. -H. Lee, J. -J. Kim, *Adv. Funct. Mater.* **2012**, 22, 855

[18] F. Atamny, A. Baiker, J. -J. Muhr, R. Nesper, *J. Anal. Chem.* **1995**, 353, 433

[19] J. Gong, G. Ma, G. Chen, *J. Mater. Res.* **1996**, 11, 8

[20] M. Manciu, R. Manaila, A. Devenyi, *Fullerene. Sci. Tech.* **1994**, 2, 255

[21] C. H. B. Ng, W. Y. Fan, *J. Phys. Chem. C* **2007**, 111, 9166

[22] A. R. Kumarasinghe, W. R. Flavell, A. G. Thomas, A. K. Mallick, D. Tsoutsou, C. Chatwin, S. Rayner, P. Kirkham, S. Warren, S. Patel, P. Christian, P. O'Brien, M. Grätzel, R. Hengerer, *J. Chem. Phys.* **2007**, 127, 114703

[23] M. Zhang, H. Wang, H. Tian, Y. Gent and C. W. Tang, *Adv. Mater.* **2011**, 23, 4960

[24] Y. -q. Zheng, W. J. Potscavage, Jr., T. Komino, M. Hirade, J. Adachi, C. Adachi, *Appl. Phys. Lett.* **2013**, 102, 143304

[25] G. Chen, H. Sasabe, Z. Wang, X.- F. Wang, Z. Hong, Y. Yang, J. Kido, *Adv. Mater.* **2012**, 24, 2768

[26] X. Xiao, J. D. Zimmerman, B. E. Lassiter, K. J. Bergemann, S. R. Forrest, *Appl. Phys. Lett.* **2013**, 102, 073302

[27] F. Jin, B. Chu, W. Li, Z. Su, B. Zhao, T. Zhang, X. Yan, Y. Gao, H. Wu, C.S. Lee, J. Zhu, H. Pi, J. Wang, *Org. Electron.* **2013**, 14, 1130

[28] S. Sutty, G. Williams, H. Aziz, *Org. Electron.* **2013**, 14, 2392

요약(국문초록)

유기태양전지에서 전자 받게 물질로 주로 사용되는 플러렌은 높은 광전도도를 가진다. 이로 인하여 플러렌층 내부에서 빛을 받아 형성된 엑시톤은 내부에 분포하는 전기장에 의하여 전자와 정공으로 쉽게 분리된다. 이러한 광전도 현상을 쇼트키 태양전지를 통하여 세 가지 방법으로 분석하였다. 첫 번째 방법은 다른 플러렌 유도체 에서도 같은 현상이 보고되는지 확인한 것이다. 플러렌 유도체중 가장 대표적인 C_{60}과 C_{70}을 비교하였을 때, 모두에서 광전도 현상이 관찰되었으며 인가전압에 선형적으로 의존하여 증가함을 확인하였다. 두 번째 방법은 계면층을 통하여 전극의 일함수를 변화시고, 그 양상을 광전도를 이용하여 분석한 것이다. 축전용량-전압 특성을 통하여 측정된 빌트인 포텐셜은 광전도를 통하여 계산된 빌트인 포텐셜과 일치하였다. 세 번째 방법은 X-선 분석을 통하여 CuI가 배향층으로 삽입되었을 때의 변화를 관찰한 것이다. CuI가 배항층으로 삽입되었을 때, 플러렌의 결정도가 증가하였고 면심입방구조의 (111)면의 발달이 관찰되었다. 이 효과를 쇼트키 태양전지에 적용한 결과 최대 93.5%의 광전도도 증가를 보였다. 5.2%의 효율이 보고된 저농도 전자 주개 유기태양전지에 위의 결과를 접목시켜 6.2%의 효율을 달성하였다.

주요어: 광전도, 플러렌, 쇼트키 태양전지, 빌트인 포텐셜, 축전용량-전압 특성, X-선 분석, CuI, 배향, 저농도 전자주개 유기태양전지

학번: 2012-20638